Parental Origin of *Gsα* Inactivation Differentially Affects Bone Remodeling in a Mouse Model of Albright Hereditary Osteodystrophy

Patrick McMullan,[1,2,3] Peter Maye,[2,3] Qingfen Yang,[1,2,3] David W. Rowe,[2,3] and Emily L. Germain-Lee[1,2,3,4] (iD)

[1]Department of Pediatrics, University of Connecticut School of Medicine, Farmington, CT, USA
[2]Department of Reconstructive Sciences, University of Connecticut School of Dental Medicine, Farmington, CT, USA
[3]Center for Regenerative Medicine and Skeletal Development, University of Connecticut School of Dental Medicine, Farmington, CT, USA
[4]Albright Center, Division of Pediatric Endocrinology, Connecticut Children's, Farmington, CT, USA

ABSTRACT

Albright hereditary osteodystrophy (AHO) is caused by heterozygous inactivation of *GNAS*, a complex locus that encodes the alpha-stimulatory subunit of heterotrimeric G proteins (Gsα) in addition to *NESP55* and *XLαs* due to alternative first exons. AHO skeletal manifestations include brachydactyly, brachymetacarpia, compromised adult stature, and subcutaneous ossifications. AHO patients with maternally-inherited *GNAS* mutations develop pseudohypoparathyroidism type 1A (PHP1A) with resistance to multiple hormones that mediate their actions through G protein-coupled receptors (GPCRs) requiring Gsα (eg, parathyroid hormone [PTH], thyroid-stimulating hormone [TSH], growth hormone–releasing hormone [GHRH], calcitonin) and severe obesity. Paternally-inherited *GNAS* mutations cause pseudopseudohypoparathyroidism (PPHP), in which patients have AHO skeletal features but do not develop hormonal resistance or marked obesity. These differences between PHP1A and PPHP are caused by tissue-specific reduction of paternal Gsα expression. Previous reports in mice have shown loss of *Gsα* causes osteopenia due to impaired osteoblast number and function and suggest that AHO patients could display evidence of reduced bone mineral density (BMD). However, we previously demonstrated PHP1A patients display normal-increased BMD measurements without any correlation to body mass index or serum PTH. Due to these observed differences between PHP1A and PPHP, we utilized our laboratory's AHO mouse model to address whether Gsα heterozygous inactivation differentially affects bone remodeling based on the parental inheritance of the mutation. We identified fundamental distinctions in bone remodeling between mice with paternally-inherited (*GnasE1+/−p*) versus maternally-inherited (*GnasE1+/−m*) mutations, and these findings were observed predominantly in female mice. Specifically, *GnasE1+/−p* mice exhibited reduced bone parameters due to impaired bone formation and enhanced bone resorption. *GnasE1+/−m* mice, however, displayed enhanced bone parameters due to both increased osteoblast activity and normal bone resorption. These in vivo distinctions in bone remodeling between *GnasE1+/−p* and *GnasE1+/−m* mice could potentially be related to changes in the bone microenvironment driven by calcitonin-resistance within *GnasE1+/−m* osteoclasts. Further studies are warranted to assess how Gsα influences osteoblast–osteoclast coupling. © 2021 The Authors. *JBMR Plus* published by Wiley Periodicals LLC on behalf of American Society for Bone and Mineral Research.

KEY WORDS: GENETIC ANIMAL MODELS; OSTEOBLASTS; OSTEOCLASTS; MOLECULAR PATHWAYS – REMODELING; DISEASES AND DISORDERS OF/RELATED TO BONE – OTHER; BONE; *Gnas*

Introduction

Fuller Albright and colleagues[1] identified a group of patients who presented with a "short, thickset figure" and biochemical abnormalities that included hypocalcemia and hyperphosphatemia. Further analysis revealed that these patients displayed a blunted physiologic response to parathyroid hormone (PTH) administration that included reduced urinary cyclic adenosine monophosphate (cAMP) and phosphate excretion.[1] Because these patients displayed typical biochemical features of hypoparathyroidism (low serum calcium with elevated serum phosphate levels) and similar patients were later shown to have elevated PTH levels due to end-organ resistance, this disorder was termed "pseudohypoparathyroidism" (PHP).[1] Future

monitoring of similar patients by Albright and colleagues[2] led to the identification of a patient who presented with the same physical features of PHP but displayed normal serum calcium and phosphate. In addition, this patient exhibited a normal phosphaturic response to PTH administration and thus the disorder was termed "pseudopseudohypoparathyroidism" (PPHP).[2] Given that PHP and PPHP share a unique cluster of physical features, which include shortened adult stature, brachydactyly, brachymetacarpia, and the formation of subcutaneous ossifications, these skeletal manifestations are collectively referred to as Albright hereditary osteodystrophy (AHO) (for review see [3-8]).[1-9]

AHO is caused by the heterozygous inactivation of *GNAS*, the gene that encodes the α-stimulatory subunit (Gsα) of G protein-coupled receptors (GPCRs) and that is required for appropriate signal transduction of multiple hormones to activate adenylyl cyclase.[3-5,7-9] The *GNAS* locus is very complex given that it encodes not only Gsα but also neuroendocrine secretory protein 55 (*NESP55*) and extra-large alpha-stimulatory subunit (*XL*αs) through the use of alternative first exons.[3-5,7-9] Furthermore, the *GNAS* locus is highly complex in that it is controlled by genomic imprinting, which can lead to partial transcriptional repression of one parental allele.[3-5,7-10] Consequently, AHO patients can display a distinct subset of extraskeletal features dependent upon the inheritance pattern of their acquired mutation. Patients with mutations on the maternally-inherited allele develop PHP type 1A (PHP1A) and display resistance to multiple hormones that mediate their actions through GPCRs requiring Gsα (eg, PTH, thyroid-stimulating hormone [TSH], growth hormone–releasing hormone [GHRH], calcitonin, luteinizing hormone [LH]/follicle-stimulating hormone [FSH]),[5,10-19] as well as have severe obesity.[20] Alternatively, patients with *GNAS* mutations on the paternally-inherited allele develop PPHP and display AHO skeletal features without exhibiting hormonal resistance[5,10-19] or severe obesity.[20] The presence of hormonal resistance within PHP1A has been shown to be due to tissue-specific reduction of paternal Gsα expression within certain endocrine organs such as the pituitary,[21] thyroid,[14,17-19] gonads,[17] and renal cortex.[3,19,22,23] Based on mouse models, the severe obesity associated with PHP1A is most likely secondary to reduced paternal Gsα expression in the dorsomedial nucleus of the hypothalamus.[24,25] It is critical, however, to acknowledge that genomic imprinting does not occur within all tissues. Rather, Gsα has been confirmed to be biallelically expressed in tissues and cell types such as the skin, heart, white adipocytes, and chondrocytes.[19,23,26-29] This biallelic expression in certain tissues and cell types is evident by the fact that PPHP and PHP1A patients share similar skeletal manifestations such as shortened adult stature and brachydactyly (which are proposed to be caused by accelerated chondrocyte differentiation due to impaired PTH/PTHrP signaling[26,30,31]) and subcutaneous ossification formation (which is potentially thought to originate from the accelerated osteogenic differentiation of cell types within the dermis and subcutaneous tissue).[32-35]

In the context of skeletal development, Gsα has been shown to serve an essential role in maintaining bone homeostasis by regulating osteoblast and osteocyte function.[36-41] Conditional deletion of Gsα specifically within mesenchymal (*Prx1-CRE*[37]), osteoblast (both *Osx-CRE*[39] and *Col1a-CRE*[36]), and osteocyte (*Dmp1-CRE*[40,41]) lineages led to a reduction in cortical and trabecular bone quality due to decreases in osteoblast number and function.[36-41] Previous reports have suggested evidence of biallelic expression of Gsα from whole human skull and femur

tissue samples[27]; however, no analysis of Gsα expression within specific cell types within the bone (osteoblast, osteoclast, or osteocyte) have been evaluated to date. These findings would suggest that AHO patients could display evidence of reduced bone mineral density (BMD) and potentially be at an elevated risk of fracture. Paradoxically, however, we found that PHP1A patients display normal to increased BMD without any correlation to body mass index (BMI) or serum PTH measurements.[42] These data suggest that the enhanced BMD within PHP1A subjects may be attributed to underlying changes in osteoblast and/or osteoclast function during the bone remodeling process and that these changes could potentially be the result of Gsα imprinting within specific cell types in the bone microenvironment. In addition, early evidence in our mouse model suggested that these changes could be driven by underlying abnormalities in the bone remodeling process, specifically decreased osteoclast activity.[19]

Our AHO mouse model, generated by targeted disruption of exon 1 of *Gnas*[19,43] (*Gnas E1+/−*) recapitulates many of the hormonal and metabolic features that are observed clinically among AHO patients; these features were shown to be due to Gsα imprinting.[19] This model also recapitulates skeletal features of AHO including the formation of subcutaneous ossifications that occur due to Gsα haploinsufficiency.[19,32] Initial skeletal characterization of this model did not identify significant changes in femur trabecular bone volume or osteoblast number of *Gnas E1+/−* mice compared to wild-type (WT) at 5 months or 1 year of age.[19] However, our initial studies of the skeletal characterization did not separate *Gnas E1+/−* mice based upon maternally-inherited (*Gnas E1+/−m*) or paternally-inherited (*Gnas E1+/−p*) mutations; additionally, these analyses did not evaluate the cortical bone quality of *Gnas E1+/−* or WT mice, which is a significant contributor to overall BMD. A subsequent study by Ramaswany and colleagues[44] utilizing our AHO mouse model provided evidence of distinct changes in cortical bone architecture among adult *Gnas E1+/−p* and *Gnas E1+/−m* mice due to changes in endosteal osteoclast number. At 2 weeks of age, both *Gnas E1+/−m* and *Gnas E1+/−p* mice displayed reduced cortical bone thickness and bone volume/total volume (BV/TV) as measured by micro–computed tomography (μCT) compared to WT. μCT analysis at 3 and 9 months revealed *Gnas E1+/−p* mice maintained these reduced cortical bone parameters; however, *Gnas E1+/−m* mice displayed an elevated cortical bone thickness and BV/TV, which were comparable to WT. These distinctions in cortical bone quality among *Gnas E1+/−* mice were found to correlate directly with changes in the number of osteoclasts on the endocortical surface; *Gnas E1+/−p* mice displayed an elevated number of endocortical osteoclasts, whereas *Gnas E1+/−m* displayed a similar number of endocortical osteoclasts compared to littermate controls.[44] This observed inheritance-specific variation in osteoclast number between *Gnas E1+/−* mice in vivo warrants a deeper investigation into identifying the role of Gsα in regulating osteoblast–osteoclast coupling during the bone remodeling process.

The purpose of this work was to identify whether Gsα heterozygous inactivation can differentially affect osteoblast activity and bone formation based upon the inheritance pattern of the *Gnas* mutation. We provide evidence showing that both *Gnas E1+/−m* and *Gnas E1+/−p* mice have a reduction in total osteoblasts on the bone surface when compared to WT. However, *Gnas E1+/−m* osteoblasts displayed substantially elevated bone formation activity when compared to both WT and *Gnas E1+/−p* in vivo. This elevated activity within *Gnas E1+/−m* mice directly

correlated with evidence of elevated cortical and trabecular bone architecture when compared to *Gnas E1+/−p* mice. We also provide evidence that these observed changes in osteoblast activity in vivo are not driven by cell-autonomous changes in *Gnas E1+/−m* osteoblasts. Instead, these changes may be secondary to partial resistance to calcitonin, a G protein-coupled hormone, within the osteoclast lineage, consistent with the BMD findings that we have previously observed in PHP1A patients.[42] Therefore, these findings correlate with our previous clinical observations and are the first to provide direct evidence of *Gsα* differentially influencing bone remodeling by affecting osteoblast–osteoclast interactions based upon the inheritance pattern of the *Gsα* mutation. In addition, our results further implicate that calcitonin signaling within the osteoclast may serve a physiologic role in regulating bone formation.

Materials and Methods

Generation and maintenance of mice

The generation of mice carrying a targeted disruption of exon 1 of *Gnas* (*Gnas E1+/−*) was described previously.[19,32] Mice were maintained on a pure 129SvEv background and were genotyped by PCR analysis. Each 20-μL reaction was performed with 2 μL DNA, 3 μL of 10× Standard Taq Reaction Buffer (New England BioLabs, Ipswich, MA, USA), 0.1 μL Taq Polymerase (New England BioLabs), 40μM of *Gnas* Forward, *Gnas* Reverse, and *Neo1* primers (sequences below), 10μM of deoxynucleoside triphosphate (dNTP) mix (Promega, San Luis Obispo, CA, USA), and 18 μL of InVitrogen Ultrapure Distilled Water (Thermo Fisher Scientific, Waltham, MA, USA). Reaction parameters were carried out as follows: 95°C for 5 minutes, 34 cycles of: (i) 95°C for 30 seconds; (ii) 60°C for 30 seconds; (iii) 72°C for 30 seconds, and two holds of 72°C for 5 minutes.

All mice that carry a mutant maternal *Gnas* allele are hereafter referred to as *Gnas E1+/−m* and those with a mutant paternal allele as *Gnas E1+/−p*. *Gnas+/+* mice are referred to as WT. Mice were fed a standard diet of Prolab RMH2500 mouse chow (PMI Nutrition International, Brentwood, Missouri, USA) and water *ad libitum*. For each of the methods outlined, both male and female mice were utilized. All in vitro cell culture experiments were performed using both male and female 6-week-old to 9-week-old mice; however, all other experiments outlined were performed using 12-week-old mice. All mouse protocols were carried out in accordance with the standards of the UConn Health Animal Care and Use Committee.

The following PCR oligonucleotide primer sequences were used:

Gene	Forward (5′ → 3′)	Reverse (5′ → 3′)
Gnas	TCGTCCCCTCAGTTGGCCAC	CCTCCCAACAAATCGCACAC
Neo 1	GAATTCGCCAATGACAAGAC	

Primary bone marrow macrophage cell culture

The hind limbs of 6-week-old to 9-week-old WT and *Gnas E1+/−* mice were dissected using aseptic technique. After removing the epiphyses, the bone marrow was harvested from both femurs and tibias by flushing the marrow space with serum-free α modified essential medium (αMEM) (Gibco, Grand Island, NY, USA) using a 26G needle. The entire bone marrow harvested from one mouse was seeded onto a 10-cm² tissue culture-treated dish in αMEM with 10% fetal bovine serum (FBS) (Gibco) and 1% penicillin/streptomycin (Gibco). The following day, nonadherent cells were collected and underwent Ficoll-Hypaque gradient centrifugation to isolate bone marrow macrophages (BMMs). To promote osteoclast differentiation, BMMs were cultured in αMEM with 10% FBS, 1% penicillin/streptomycin, as well as 30 ng/mL recombinant murine macrophage-colony stimulating factor (m-CSF; PeproTech, Rocky Hill, NJ, USA) and 45 ng/mL recombinant murine receptor activator of nuclear factor–κB (RANK) ligand (RANKL; PeproTech) for 5 days. For chromogenic tartrate-resistant acid phosphatase (TRAP) staining, BMM cultures were seeded at 5×10^3 cells/well of a 96-well dish. All additional in vitro BMM experiments were performed with 1×10^5 cells/well in a 12-well dish. For staining analyses, BMM cultures were fixed with 5% glutaraldehyde (Thermo Fisher) in phosphate buffered saline (PBS) for 10 minutes at room temperature, permeabilized for 60 minutes at room temperature using 0.3% Triton-X (Thermo Fisher) and 0.1% bovine serum albumin (BSA) (Thermo Fisher) in PBS with calcium and magnesium. Cells were stained with tetramethylrhodamine isothiocyanate (TRITC)-conjugated phalloidin (Sigma-Aldrich, St. Louis, MO, USA) for 45 minutes, followed by 4′,6-diamidino-2-phenylindole (DAPI) (Sigma-Aldrich) for 10 minutes. BMM cultures were visualized by fluorescent microscopy utilizing both TRITC and DAPI filters. Following fluorescent image acquisition, BMM cultures were subsequently stained for chromogenic TRAP using a Leukocyte Acid Phosphatase Kit (Sigma-Aldrich; 387A-1KT) for 60 minutes at 37°C as recommended by the manufacturer.

Primary bone marrow stromal cell culture

The hind limbs of 6-week-old to 9-week-old WT and *Gnas E1+/−* mice were dissected using aseptic technique. After removing the epiphyseal ends, the bone marrow was harvested from both femurs and tibias by flushing with a 26G needle and the number of mononucleated cells were counted using a hemocytometer. For colony forming unit (CFU) assays, 1×10^6 mononucleated cells/well were seeded into a six-well culture dish. For RNA analysis, as well as Alizarin Red and Von Kossa staining, 1×10^7 cells/well were seeded onto a six-well dish. Bone marrow stromal cells (BMSCs) were cultured for 7 days (days −7 to 0) in basal culture media (αMEM with 10% FBS and 1% penicillin/streptomycin). Following this period, BMSCs underwent osteogenic differentiation by supplementing the basal media with 50 μg/mL ascorbic acid (Thermo Fisher) and 10mM beta-glycerophosphate (Thermo Fisher) for up to 14 days (days 0–14). To monitor the number of osteoprogenitor colony formation units, alkaline phosphatase (AP) staining was completed within each well using a commercially available leukocyte AP staining kit (Sigma-Aldrich; 86R-1KT). Whole-well images were collected through brightfield microscopy and quantification of CFUs was performed using ImageJ software (NIH, Bethesda, MD, USA; https://imagej.nih.gov/ij/). In order to monitor osteogenic differentiation of WT and *Gnas E1+/−* BMSCs, cultures were fixed for 10 minutes in 4% paraformaldehyde (PFA) in PBS for Alizarin Red staining, or ice-cold 100% methanol for Von Kossa staining. Alizarin Red staining and quantification was performed using a commercially available staining kit (ScienCell, Carlsbad, CA, USA; catalog #0223). Von Kossa staining was performed by staining cultures with 4% silver nitrate solution (Thermo Fisher) and exposing cultures to 2400 kJ of ultraviolet

Table 1. Real-Time Quantitative RT-PCR Oligonucleotide Primer Sequences

Gene	Forward (5′ → 3′)	Reverse (5′ → 3′)
Alpl	AATGAGGTCACATCCATCC	CGAGTGGTAGTCACAATGC
Bglap1	TCCAAGCAGGAGGGCAATAAG	GCGTTTGTAGGCGGTCTTCAAG
Calcr	AGCCACAGCCTATCAGCACT	GACCCACAAGAGCCAGGTAA
C-fos	CGGGTTTCAACGCCGACTA	TTGGCACTAGAGACGGACAGA
Crem	CAGACTAGCACGGGGCAATAC	AGCCACACGATTTTCAAGACAT
Ctsk	GCCACGCTTCCTATCCGAAA	ACCCACATCCTGCTGTTGAG
Dmp1	CGCATCCCAATATGAAGACTG	GCTTGACTTTCTTCTGATGACTCA
Gsα	ACCAGCGCAACGAGGAGAA (Exon 1)	CCCATCCGGCGTCACTAAT (Exon 2)
Ibsp	CGCCACACTTTCCACACTCTC	CTTCCTCGTCGCTTTCCTTCAC
Nfatc1	TGGAGAAGCAGAGCACAGAC	GCGGAAAGGTGGTATCTCAA
Opg	GCAGAGACGCACCTAGCACTG	GCCAGCTGTCCGTATAAGAGT
Ramp3	GTGAGTGTGCCCAGGTATGC	CGACAGGTTGCACCACTTC
Rank	AGCAGATGCGAACCAGGAAA	ACACACTGTCGGAGGTAGGA
Rankl	CAGAAGACAGCACTCACTGCT	CATTGATGGTGAGGTGTGCAA
Sema4d	TCTTTGCTGACGTGATCCAG	CAGATCAGCCTGGCCTTTAG
Sphk1	TGAGGTGGTGAATGGGCTAATGGA	AACAGCAGTGTGCAGTTGATGAGC
Sphk2	TGGGCTGTCCTTCAACCTCATACA	AGTGACAATGCCTTCCCACTCACT
Sp7	GGATGGCGTCCTCTCTGCTTGAG	GAGGAGTCCATTGGTGCTTGAGA
Wnt10b	AGGCTTCTCCTTCCGTTCAGTTGT	ATTCCCACCCTTCCTGCTGAAGAA

All forward and reverse primer sequences are located on different exons.

In vitro salmon calcitonin, PTH 1–34, and forskolin treatment

WT and *Gnas E1+/−* BMSC or BMM cultures were treated with 1×10^{-7}M of salmon calcitonin (sCT) (R&D Systems, Minneapolis, MN, USA), 1×10^{-7}M PTH (ProSpec, East Brunswick, NJ, USA), 1×10^{-5}M of forskolin (Sigma-Aldrich) or vehicle (PBS) controls for 6 hours in serum-free αMEM.

Quantitative RT-PCR

Total RNA was extracted from BMSC and BMM cell cultures, as well as tibia diaphysis tissue samples. For cell culture experiments, adherent cells were rinsed in ice-cold nuclease-free water. Samples were subsequently exposed to 500 μL TRIzol (Invitrogen, Carlsbad, CA, USA). For tibia harvesting, the tissue samples were freshly dissected, removing the surrounding muscle and connective tissue. After scraping off the periosteum with a 10-blade scalpel, the epiphyses were removed. The remaining tibias were placed within a 200-μL pipette tip inside of a microcentrifuge tube and underwent centrifugation at 16,000*g* (14,000 rpm) for 60 seconds at 4°C. After removing the marrow, the tibias were placed into RNA Later solution (Invitrogen) and stored at −80°C. For RNA extraction, both tibiae from each mouse were placed into 1 mL of TRIzol (Invitrogen) on ice and homogenized.

To extract RNA, 200 μL of Chloroform (Sigma-Aldrich) was placed into TRIzol-exposed cell culture or homogenized tissue samples. The clear aqueous layer was isolated and was subsequently run through a Direct-zol RNA Miniprep Kit (Zymo Research, Irvine, CA, USA). The isolated RNA was treated with DNAse I (New England BioLabs) for 10 minutes at 37°C to remove any remaining genomic DNA, followed by DNAse inactivation by EDTA treatment and heat inactivation at 75°C for 10 minutes. The DNAse-treated RNA samples were then placed through a Monarch RNA Cleanup Kit (New England BioLabs) to ensure no carryover of contaminants; then, 500 ng of RNA was utilized for reverse transcription using a high capacity cDNA reverse transcription kit (Applied Biosystems, Foster City, CA, USA). Quantitative RT-PCR was performed within a 20-μL reaction, consisting of iTaq Universal SYBR Green Supermix (Bio-Rad, Hercules, California, USA), 10μM of forward and reverse primers, and 25 ng of cDNA. The specific primer sequences utilized are listed in Table 1.

μCT analysis

Analysis of femur and lumbar vertebral bone parameters were completed on *Gnas E1+/−* and WT mice using μCT (μCT 40; Scanco Medial AG, Bassersdorf, Switzerland). The lumbar vertebrae (L_4 through L_6) and femurs of WT and *Gnas E1+/−* mice were dissected to remove surrounding connective tissue and fixed in 70% ethanol at 4°C. Cortical bone parameters were measured at the femur mid-diaphysis. Trabecular bone parameters were performed at the distal metaphyseal region of the femur and the centrum of the L_5 vertebrae. μCT analysis was performed using the following parameters: voxel size of 8 μm, 55 kV, and 145 μA.

Tissue fixation, embedding, and sectioning for bone histomorphometry

Femur and lumbar vertebrae samples were harvested, immediately dissected to remove surrounding connective tissue and muscle and fixed in 10% neutral buffered formalin (NBF) (Sigma Aldrich) for 5 days at 4°C. The bones were then briefly transferred to PBS for 2 hours then placed in 30% sucrose (Sigma Aldrich) for 48 hours at 4°C. Samples were then embedded into optimal cutting temperature (OCT) compound (Sigma Aldrich) and blocks were stored at −80°C until use. Five micrometer (5-μm) undecalcified sections were utilized for histomorphometry analysis.

Dynamic histomorphometry was performed by alizarin complexone (AC) (Sigma Aldrich A-3882) and calcein (Sigma Aldrich C-0875) double-labeling, in addition to fluorescence-based AP and staining as described.[45] Briefly, WT and *Gnas E1+/−* mice were administered alizarin complexone (AC) by intraperitoneal injection (dose 30 mg/kg) 7 days prior to euthanasia by CO_2 asphyxiation according to Institutional Animal Care and Use Committee (IACUC) regulations. These same mice were additionally administered calcein (dose 10 mg/kg) 2 days prior to euthanasia. Tissue specimens of undecalcified distal femur and lumbar vertebrae were imaged using a Ziess Axioscan Z1 high speed automated image acquisition system (Carl Zeiss Microscopy, Inc., Dublin, CA, USA; Cat#440640-9903-000) and a high resolution camera (AxioCam HRm; Carl Zeiss Microscopy, Inc.). Trabecular mineral apposition rate (MAR) analyses, and AP and TRAP measurements were calculated using a computer-automated dynamic histomorphometry image analysis software as described.[45] Additionally, distal femur sections were stained with a leukocyte acid phosphatase staining kit (Sigma-Aldrich; 387A-1KT) in order to visualize osteoclasts on the bone surface, and were counterstained with Aniline Blue to stain bone tissue. Endocortical MAR and chromogenic TRAP analysis was performed using the standard histomorphometry analysis software OsteoMetrics (OsteoMetrics, Decatur, GA, USA).

Serum and plasma analyses

Serum and plasma samples were harvested from 12-week-old WT and *Gnas E1+/−* mice by cardiac puncture after fasting for 6 hours and stored at −80°C until use. Serum measurements were performed through the use of Immunodiagnostic Systems mouse serum procollagen type 1 N-terminal propeptide (P1NP) (Immunodiagnostic Systems, Gaithersburg, MD, USA; IDS AC-33F1) and serum collagen type 1 C-terminal telopeptide (CTX-1) (Immunodiagnostic Systems; AC-06F1) ELISA kits. Plasma measurement of calcitonin was performed using an ABClonal Calcitonin Plasma ELISA kit (ABclonal, Inc., Woburn, MA, USA; RK02716). All plasma and serum samples were performed in duplicate and each individual data point generated consisted of the mean value obtained from duplicate samples.

Statistical analysis

All statistical analyses were performed using GraphPad Prism, version 9 (GraphPad Software, Inc., La Jolla, CA, USA), with *p* values <0.05 to be considered as statistically significant. For all analyses observed at one discrete time point, data obtained from WT, *Gnas E1+/−p*, and *Gnas E1+/−m* mice were analyzed by a one-way ANOVA with a post hoc Tukey test for multiple comparisons. For Alizarin Red staining and RT-PCR data comparing changes in mRNA expression at multiple time points or following multiple drug treatments, a two-way ANOVA with a post hoc Tukey test for multiple comparisons was utilized.

Results

Gnas E1+/−m mice display significantly enhanced cortical and trabecular bone parameters when compared to *Gnas E1+/−p* mice

In order to identify the impact of *Gsα* heterozygous inactivation on cortical and trabecular bone architecture, we utilized our AHO mouse model generated by targeted disruption of exon 1 of *Gnas* (*Gnas E1+/−*), leading to global heterozygous inactivation of *Gsα*.[19] We utilized 12-week-old mice bred on a pure 129SvEv background, given that this specific background led most closely to recapitulating the human disorder.[19] *Gnas E1+/−m* mice are obese and shorter than their WT counterparts, exhibit hormonal resistance to PTH and TSH, have decreased fertility, and develop subcutaneous ossifications.[19] Conversely, *Gnas E1+/−p* mice are not obese and have no hormonal resistance or significant infertility, but they also develop subcutaneous ossifications as in the PPHP human counterpart.[19,32,33] Quantitative RT-PCR of bone-marrow flushed tibia specimens from male and female mice revealed that *Gnas E1+/−* mice displayed a significant reduction in *Gsα* mRNA expression when compared to WT (Fig. 1A). No significant variations in *Gsα* mRNA expression were observed when comparing *Gnas E1+/−p* to *Gnas E1+/−m* mice (Fig. 1A).

The cortical bone architecture of *Gnas E1+/−* and WT mice was analyzed at the mid-diaphysis of the femur by μCT (Fig. 1B). All analyses were monitored in both male and female mice, given that previous reports only compared changes in skeletal parameters between male *Gnas E1+/−* and WT mice.[44] Male *Gnas E1+/−* mice (both *Gnas E1+/−p* and *Gnas E1+/−m*) displayed a significant reduction in femur length when compared to WT (Fig. 1C); no significant variations were seen in females (*p* = 0.06). Despite evidence of reduced femur lengths, *Gnas E1+/−m* and *Gnas E1+/−p* mice displayed no significant variations in the ratio of cortical area to total bone area (CA:TA) when compared to WT (Fig. 1D), and therefore we were able to make direct comparisons in cortical bone thickness and architecture between each genotype. These analyses revealed male *Gnas E1+/−p* mice displayed significant reductions in cortical bone thickness (Fig. 1E), cortical mask (area between periosteal and endosteal surfaces) (Fig. 1F), and periosteal and endocortical perimeters (Fig. 1G,H) when compared to *Gnas E1+/−m* and WT mice. Female *Gnas E1+/−p* mice similarly displayed reduced cortical bone parameters when compared to *Gnas E1+/−m* mice but only displayed a reduction in cortical mask and periosteal perimeter when compared to WT. These data correlate with earlier findings in our mouse model[19] (including those seen in *Gnas E1+/−* mice bred on a hybrid 129SvEv x CD-1 background) and further confirm that adult *Gnas E1+/−p* mice display reduced cortical bone parameters, whereas *Gnas E1+/−m* mice display normal to increased cortical bone parameters when compared to WT.[44]

In conjunction with monitoring changes in cortical bone, we analyzed the trabecular architecture of *Gnas E1+/−* and WT mice by μCT at the distal femur (Fig. 2A) and lumbar vertebrae (Fig. 2B). When comparing the femurs of *Gnas E1+/−p* mice to WT, we did not observe a significant trabecular bone phenotype. No significant variations in BV/TV, trabecular number or trabecular spacing were observed in female mice (Fig. 2C–F); male *Gnas E1+/−p* mice did display a reduction in trabecular thickness when compared to WT but displayed no variations in BV/TV, trabecular number or trabecular spacing. However, the comparison of female *Gnas E1+/−m* mice to WT displayed an elevated BV/TV and trabecular number and a reduction in trabecular spacing (Fig. 2C–E). No significant variations were observed between male *Gnas E1+/−m* and WT mice. When comparing *Gnas E1+/−m* and *Gnas E1+/−p* mice, we observed *Gnas E1+/−m* mice display a significantly elevated increase in trabecular bone thickness (Fig. 2D) but displayed no significant variations in BV/TV, trabecular thickness, or trabecular number. μCT analysis of the lumbar vertebrae revealed no significant variations in trabecular bone parameters between *Gnas E1+/−m*, *Gnas E1+/−p*, and WT mice (Fig. 2G–J). Collectively, these data further highlight the
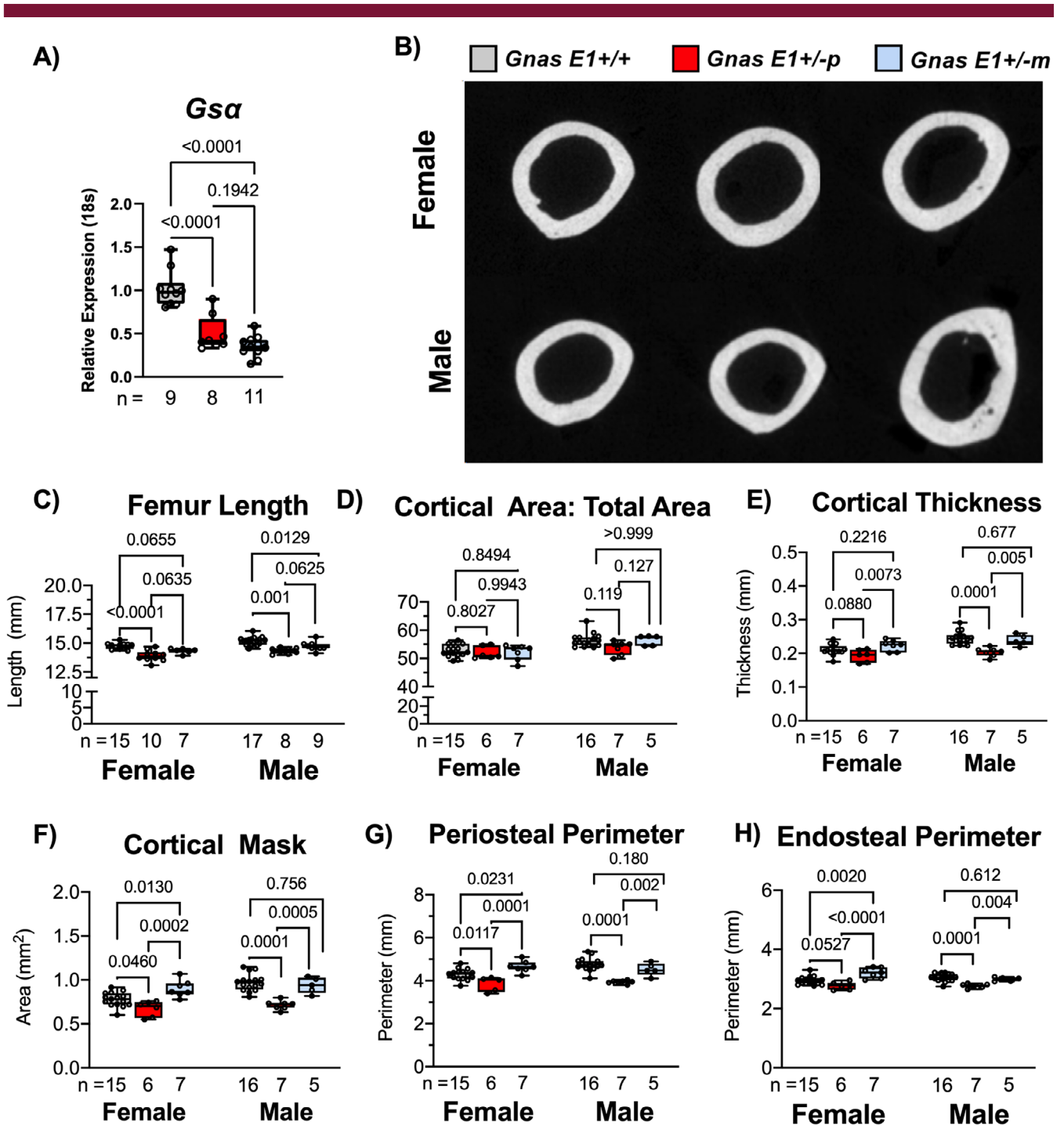
Fig 1. Cortical bone parameters are dependent upon inheritance pattern of *Gsα* mutation. (*A*) Gsα mRNA expression is reduced within flushed tibia samples of *Gnas E1+/−m* and *Gnas E1+/−p* mice compared to WT. (*B*) Representative cross-sectional images of cortical bone of distal femur across both WT and *Gnas E1+/−* animals. (*C*) Both male and female *Gnas E1+/−p* mice had a significantly reduced femur length compared to WT. Male *Gnas E1+/−m* mice also had a significantly reduced femur length compared to WT but no significant variations were observed among female *Gnas E1+/−m* and WT mice. (*D*) Phenotypic differences observed within cortical bone of both *Gnas E1+/−p* and *Gnas E1+/−m* animals are not attributed solely to decreased length, based on the lack of significant differences seen within the ratio of cortical area to total bone area; (*E–H*) Statistically significant decreases in cortical bone parameters were observed in *Gnas E1+/−p* compared to *Gnas E1+/−m* in both male and female animals. *Gnas E1+/−p* animals demonstrated significant decreases in cortical bone parameters compared to *Gnas E1+/−m* mice, and displayed normal to reduced parameters when compared to WT. Conversely, *Gnas E1+/−m* demonstrated normal to increased cortical bone parameters compared to WT. Sample size per genotype per experiment is listed on each bar graph. All statistical tests completed using ANOVA with post-hoc Tukey test for multiple comparisons, and *p* values are displayed for each comparison.
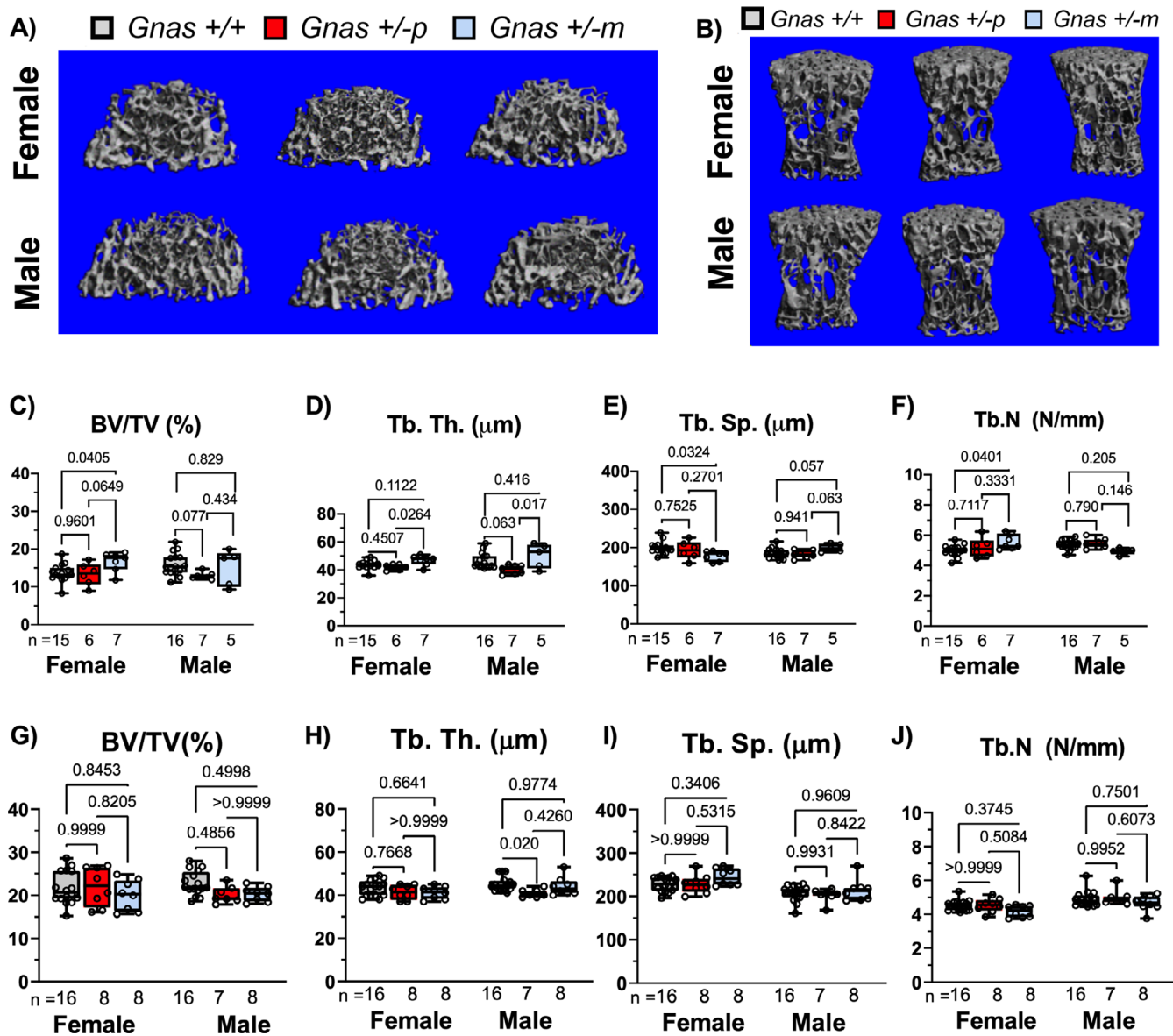
Fig 2. Femur and vertebral trabecular bone parameters are mildly influenced by *Gsα* heterozygous inactivation. Representative μCT images of trabecular bone from the (*A*) distal femur and (*B*) L$_5$ vertebrae of WT and *Gnas E1+/−* animals. (*C–F*) *Gnas E1+/−p* mice, when compared to WT, displayed no significant femur trabecular bone phenotype. However, female *Gnas E1+/−m* mice when compared to WT displayed a significantly elevated BV/TV, trabecular number, and a reduction in trabecular spacing (no variations observed between male mice). *Gnas E1+/−m* mice, when compared to *Gnas E1+/−p*, displayed a significant increase in trabecular thickness. (*G–J*) No significant differences were observed between WT and *Gnas E1+/−* mice with respect to vertebral trabecular bone parameters. Sample size per genotype per experiment is listed on each bar graph. All statistical tests completed using ANOVA with post-hoc Tukey test for multiple comparisons, and *p* values are displayed for each comparison.

presence of distinctions in both cortical and trabecular bone parameters between adult *Gnas E1+/−m* and *Gnas E1+/−p* mice, particularly within the femur.

Elevated cortical and trabecular bone parameters in *Gnas E1+/−m* mice are associated with increased osteoblastic activity in vivo

We next evaluated whether the observed differences in cortical and trabecular bone between *Gnas E1+/−m* and *Gnas E1+/−p* mice could be attributed to variations in osteoblast number or underlying osteoblast activity. To address these questions, we utilized a computer-automated fluorescent-based multiplex histomorphometry technique to label actively-mineralizing osteoblasts along the bone surface of the distal femur and lumbar vertebrae using AP staining in conjunction with calcein and alizarin complexone mineral labeling (Fig. 3*A*).[45] In addition to histomorphometry, we compared overall bone forming activity in vivo by serum P1NP measurements and gene expression analyses of osteoblast-related transcripts osteocalcin (*Bglap1*), integrin-binding sialoprotein (*Ibsp*), and dentin matrix acidic phosphoprotein 1 (*Dmp1*) by RT-PCR.
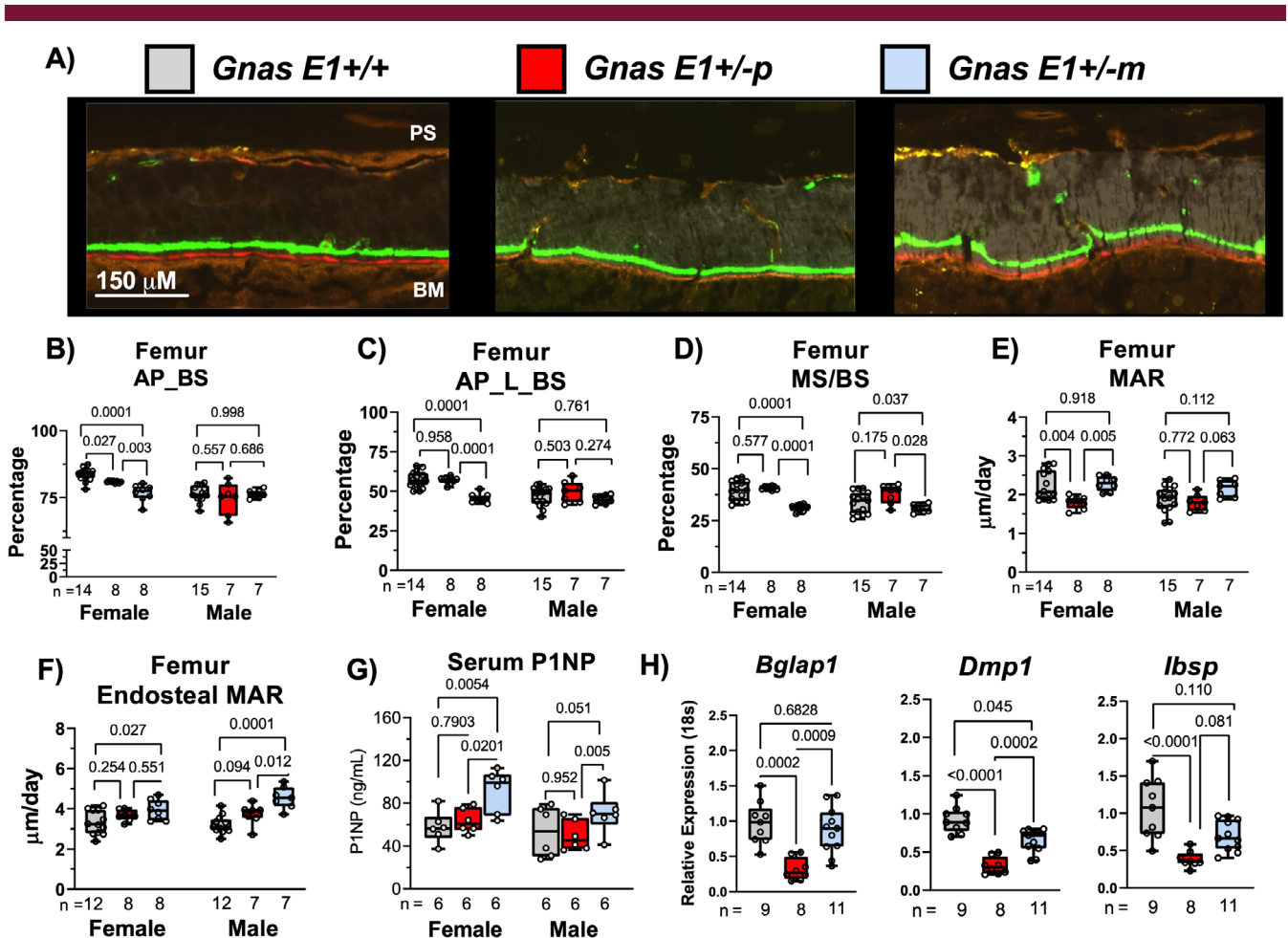
Fig 3. Enhanced cortical and trabecular bone parameters in *Gnas E1+/−m* mice are directly associated with elevated osteoblast activity despite a reduction in osteoblast number. (*A*) Representative images of undecalcified femur cortical bone sections containing calcein (green) and alizarin complexone (red) labels for dynamic histomorphometry. (*B*) Significant reductions in total AP activity on the bone surface (AP_BS) were observed within female *Gnas E1+/−p* and *Gnas E1+/−m* femur sections compared to WT. No significant differences were observed in male specimens across all genotypes. (*C*) *Gnas E1 +/−m* mice displayed a reduction in the total number of actively mineralizing osteoblasts (AP_L_BS) when compared to WT and *Gnas E1+/−p* mice. (*D*) Dynamic histomorphometry on the femur trabecular surface revealed *Gnas E1+/−m* mice displayed a significant reduction in MS/BS within the femur when compared to both WT and *Gnas E1+/−p* mice (*E*) Female *Gnas E1+/−p* mice had a significantly reduced mineral apposition rate compared to both *Gnas E1+/−m* and WT. MAR among *Gnas E1+/−m* was comparable to WT. We observed no significant variations within male mice. (*F*) *Gnas E1+/−m* mice displayed a significantly increased MAR on the femoral endosteal surface compare to WT mice, as well as when compared to *Gnas E1+/−p* mice for males. (*G*) Serum P1NP levels were significantly elevated within *Gnas E1+/−m* mice compared to *Gnas E1+/−p* and WT samples. No significant variations were observed between *Gnas E1+/−p* and WT samples. (*H*) *Bglap1*, *Dmp1*, and *Ibsp* mRNA expression in flushed tibia specimens were significantly reduced in *Gnas E1+/−p* male and female mice compared to WT. *Gnas E1+/−m* samples displayed no significant reduction in *Bglap* and *Ibsp* expression when compared to WT but displayed a reduction in *Dmp1* expression. *Gnas E1+/−m* samples, when compared to *Gnas E1+/−p*, displayed a significantly elevated *Bglap1* and *Dmp1* expression, but displayed no significant variations in *Ibsp* expression. Sample size per genotype per experiment is listed on each bar graph. All statistical tests completed using ANOVA with post-hoc Tukey test for multiple comparisons, and *p* values are displayed for each comparison. AP_BS = Alkaline phosphatase positive cells on the bone lining surface (indicative of total number of osteoblasts); AP_L_BS = Alkaline phosphatase positive cells on the bone lining surface superimposed over a mineral label (indicative of actively mineralizing osteoblasts).

Although histomorphometric analyses were performed using both male and female mice, we primarily observed significant variations in overall bone remodeling within female *Gnas E1 +/−* and WT mice. In particular, we observed both female *Gnas E1+/−m* and *Gnas E1+/−p* mice displayed a statistically significant reduction in the presence of osteoblasts along the bone surface (AP_BS) when compared to WT at both the distal femur (Fig. 3B) and lumbar vertebrae (Supplemental Fig. S1A). Despite female *Gnas E1+/−m* mice displaying enhanced cortical and trabecular bone architecture, these mice displayed a reduction in

the number of actively mineralizing osteoblasts (measured by both AP+ populations on the bone surface superimposed over a mineral label [AP_L_BS] and MS/BS) within the distal femur (Fig. 3C,D) and lumbar vertebrae (Supplemental Fig. S1B,C) when compared to both *Gnas E1+/−p* and WT mice.

We utilized calcein and alizarin complexone double labeling to quantify the MAR along three separate bone surfaces in *Gnas E1+/−* and WT mice: the trabecular surfaces of the distal femur, the endocortical surface of the femur, and the trabecular surface of the lumbar vertebrae. Along the femur trabecular surface,

female *Gnas E1+/−p* mice displayed a significant reduction in MAR when compared to both *Gnas E1+/−m* and WT (Fig. 3E). Alternatively, *Gnas E1+/−m* mice displayed MAR values that were comparable to WT despite displaying an overall reduction in the number of active osteoblasts on the bone surface. No significant variations in trabecular MAR were observed in male mice (Fig. 3E). Subsequent analysis of MAR along both the femur endocortical surface (Fig. 3A,F) and the lumbar vertebrae trabecular surface (Supplemental Fig. S1D) revealed that *Gnas E1+/−m* mice displayed a significantly elevated MAR compared to WT, whereas no significant differences were observed between *Gnas E1+/−p* and WT mice at either of these two locations. Complementary to our histomorphometry findings, female *Gnas E1+/−m* mice displayed significantly elevated serum P1NP measurements when compared to both *Gnas E1+/−p* and WT (Fig. 3G). Male *Gnas E1+/−m* mice also displayed elevated P1NP levels when compared to *Gnas E1+/−p* mice, but were not significantly higher than WT ($p = 0.051$). No significant differences were observed between *Gnas E1+/−p* and WT mice in both males and females. Quantitative RT-PCR analysis of flushed tibia specimens from male and female mice displayed *Gnas E1+/−p* mice having a significant reduction in *Bglap1* ($p < 0.001$), *Dmp1* ($p < 0.001$), and *Ibsp* ($p < 0.001$) (Fig. 3H) mRNA expression when compared to WT. These data complement our histologic findings in the femur and lumbar vertebrae, and further suggest evidence of reduced osteoblast activity within *Gnas E1+/−p* mice compared to WT. However, *Gnas E1+/−m* mice displayed no significant variations in *Bglap1* ($p = 0.683$) and *Ibsp* ($p = 0.110$) mRNA expression when compared to WT but did have a reduction in *Dmp1* expression ($p = 0.045$). In addition, *Gnas E1+/−m* mice displayed a significant increase in *Bglap1* ($p = 0.0009$) and *Dmp1* ($p = 0.0002$) expression when compared to *Gnas E1+/−p* but displayed no significant variation in *Ibsp* ($p = 0.081$) expression. These data suggest that despite an overall reduction in the total number of active osteoblasts within the femoral and vertebral bone surface of *Gnas E1+/−* mice, the enhanced cortical and trabecular bone parameters specifically observed within *Gnas E1+/−m* mice can be attributed to an increase in the total matrix production per osteoblast in vivo when compared to *Gnas E1+/−p* mice.

Given these observed distinctions in osteoblast activity in vivo, we next isolated primary BMSCs from both male and female mice to identify whether there were any significant variations in the transcriptional activity or osteogenic differentiation within the osteoprogenitor populations of *Gnas E1+/−m* and *Gnas E1+/−p* mice (Fig. 4). When cultured in basal media (αMEM with 10% FBS), no significant variations were observed between the osteoprogenitor populations of *Gnas E1+/−* and WT cultures, as measured by the number of AP+ CFUs (Fig. 4A,B). When supplemented with osteogenic inducing media for 7 and 14 days, no significant variations in osteogenic differentiation or mineralization were observed between *Gnas E1+/−* and WT cultures as measured by Alizarin Red or Von Kossa staining (Fig. 4A,C). However, gene expression analyses of *Gsα* and osteogenic-related genes *Alpl* (AP), *Sp7* (Osterix), and *Bglap1* were also performed within cultures in basal media (day 0) and following 7 and 14 days of osteogenic differentiation (Fig. 4D–G). At each time point, both *Gnas E1+/−m* and *Gnas E1+/−p* cultures displayed significant reductions in *Gsα* mRNA expression (Fig. 4D) when compared to WT cultures. When cultured in basal media, no significant variations in *Alpl*, *Sp7*, or *Bglap1* were observed between *Gnas E1+/−* and WT cultures (Fig. 4E–G).

However, *Gnas E1+/−m* cultures after 7 days of osteogenic differentiation displayed a significant upregulation in *Alpl* (Fig. 4E) and *Sp7* (Fig. 4F) mRNA expression when compared to WT and *Gnas E1+/−p*. Additionally, after 14 days of osteogenic differentiation, *Gnas E1+/−m* BMSCs displayed an increase in *Alpl* (Fig. 4E) and *Bglap1* (Fig. 4G) mRNA expression compared to WT and *Gnas E1+/−p* cultures. Although *Gnas E1+/−m* BMSCs display elevated osteogenic transcriptional activity in vitro, the lack of a mineralization or differentiation phenotype in vitro suggests that the observed changes in osteoblast activity within *Gnas E1+/−m* mice in vivo may not be solely driven by cell autonomous changes in osteogenic differentiation capacity, but instead, could be attributed to local changes within the bone microenvironment.

Gsα heterozygous inactivation differentially affects transcriptional activity of osteoclast-secreted anabolic coupling factors in vitro

In addition to assessing osteoblast activity, we also assessed whether *Gsα* heterozygous inactivation differentially influences osteoclast differentiation and structural morphology. In vitro analysis of primary BMM cultures from male and female mice revealed both *Gnas E1+/−m* and *Gnas E1+/−p* cultures had elevated rates of osteoclastogenesis when compared to WT as measured by chromogenic tartrate-resistant acid phosphatase (TRAP) staining (Fig. 5A,B). Fluorescent microscopy using phalloidin revealed *Gnas E1+/−m* and *Gnas E1+/−p* osteoclasts displayed appropriate actin ring morphology and were significantly larger in overall surface area when compared to WT (Fig. 5A,B). Quantitative RT-PCR revealed *Gnas E1+/−m* and *Gnas E1+/−p* BMM cultures displayed a significant upregulation of *Rank* (Fig. 5C) and *Calcr* (Fig. 7A) mRNA expression when compared to WT, but displayed no significant variations in *Nfatc1* or *Ctsk* mRNA expression (Fig. 5C). Collectively, these data correlate with previous reports suggesting *Gsα* serves as a negative regulator of osteoclastogenesis and that parental inheritance of the *Gsα* mutation does not selectively influence osteoclastogenesis in vitro.[44,46]

In addition to evaluating osteoclastogenesis in vitro, we wanted to assess whether the observed distinctions in bone formation between *Gnas E1+/−m* and *Gnas E1+/−p* mice in vivo could be attributed to modifications in osteoclast secreted bone coupling factors. We examined four growth factors that are released by osteoclasts and have been shown to influence bone formation: *Semaphorin 4d* (*Sema4d*), *Sphingosine Kinase 1* (*Sphk1*), *Sphingosine Kinase 2* (*Sphk2*), and *Wnt10b* (Fig. 5D).[47–52] *Gnas E1+/−p* BMM cultures displayed no significant variations in transcriptional activity when compared to WT. However, *Gnas E1+/−m* BMM cultures displayed significantly enhanced *Sphk1* transcriptional activity when compared to WT ($p = 0.001$), but were not statistically significant when compared to *Gnas E1+/−p* cultures ($p = 0.059$) (Fig. 5D). *Sphk1* and Sphingosine 1-phosphate (S1P) signaling within the osteoclast has been well recognized to promote osteoblast function in vivo.[47–52] Therefore, these data underscore that the distinctions in bone forming activity between *Gnas E1+/−m* and *Gnas E1+/−p* mice could be attributed to variations in osteoblast–osteoclast coupling interactions within the bone microenvironment and that one possible mechanism for these distinctions in coupling may be secondary to S1P-related signaling.
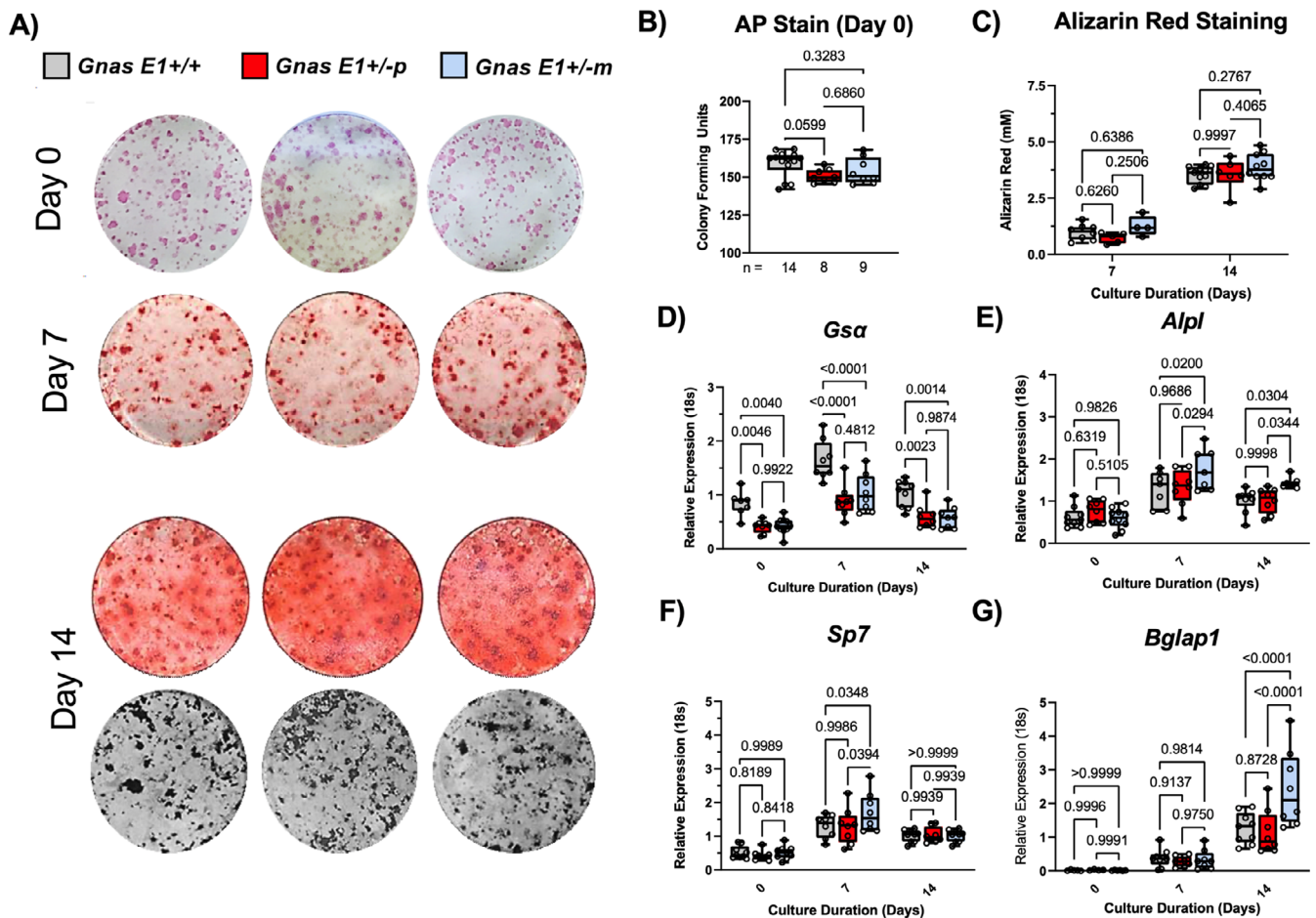
Fig 4. Inheritance pattern of *Gsα* mutation does not differentially influence osteoprogenitor differentiation in vitro. (*A*) Representative entire-well images of: alkaline phosphatase positive (AP+) colony formation units within primary BMSCs at day 0 from male and female mice; Alizarin Red staining to detect calcium deposition on culture days 7 and 14; and Von Kossa staining to detect phosphate on culture day 14. (*B*) Both *Gnas E1+/−m* and *Gnas E1+/−p* demonstrated no significant differences within the osteoprogenitor populations compared to WT BMSCs as measured by AP colony forming unit assays. (*C*) *Gnas E1+/−* and WT BMSCs following 7 and 14 days of osteogenic differentiation displayed no significant variations in Alizarin Red staining absorbance. (*D-G*) Both *Gnas E1+/−m* and *Gnas E1+/−p* BMSCs displayed significant reductions in *Gsα* expression at each time point when compared to WT. Prior to osteogenic differentiation, no significant differences were observed in (E) *Alpl*, (F) *Sp7*, and (G) *Bglap1* mRNA expression among *Gnas E1 +/−* and WT BMSCs. However, *Gnas E1+/−m* mice displayed elevated mRNA expression of (E) *Alpl* and (F) *Sp7* after 7 days of osteogenic differentiation and (E) *Alpl* and (G)*Bglap1* after 14 days of osteogenic differentiation when compared to both WT and *Gnas E1+/−p*. Sample size per genotype per experiment is listed on each bar graph. For AP+ colony assay, statistical tests were completed using a one-way ANOVA with post-hoc Tukey test for multiple comparisons. For alizarin red staining and RT-PCR analyses at multiple time points, statistical tests were completed using a two-way ANOVA with post-hoc Tukey test for multiple comparisons. Values of *p* are displayed for each comparison.

Reduced cortical and trabecular bone parameters within *Gnas E1+/−p* are attributed to enhanced osteoclast activity in vivo

In conjunction with assessing bone formation, we compared overall bone resorption between *Gnas E1+/−* and WT mice in vivo by histomorphometry at the distal femur and vertebrae, serum CTX-1 measurement, and RT-PCR to measure *Rankl* and *Opg* mRNA expression within flushed tibia samples. Histomorphometric analysis to assess osteoclast activity was performed by incubating sections with Elf97 substrate (Life Technologies, Inc., Grand Island, NY, USA; E6589), which generates a fluorescent signal when cleaved by TRAP and has been reproducibly shown

to stain osteoclasts in vivo (Fig. 6*A*),[45,53] in addition to conventional chromogenic TRAP staining to quantify osteoclast number.

Histologic analyses at the distal femur revealed that *Gnas E1+/−p* mice display elevated TRAP activity on the endosteal and periosteal surfaces when compared to both WT and *Gnas E1+/−m* mice (Fig. 6*A,B*). In addition, female *Gnas E1+/−p* mice displayed elevated total TRAP activity (TRAP_BS) (Fig. 6*C*) and active remodeling surfaces (defined as TRAP+ signals over a mineralizing surface, or TRAP_L_BS) (Fig. 6*D*) when compared to both *Gnas E1+/−m* and WT. No significant variations were observed between female *Gnas E1+/−m* and WT samples. In alignment with the observed TRAP_BS
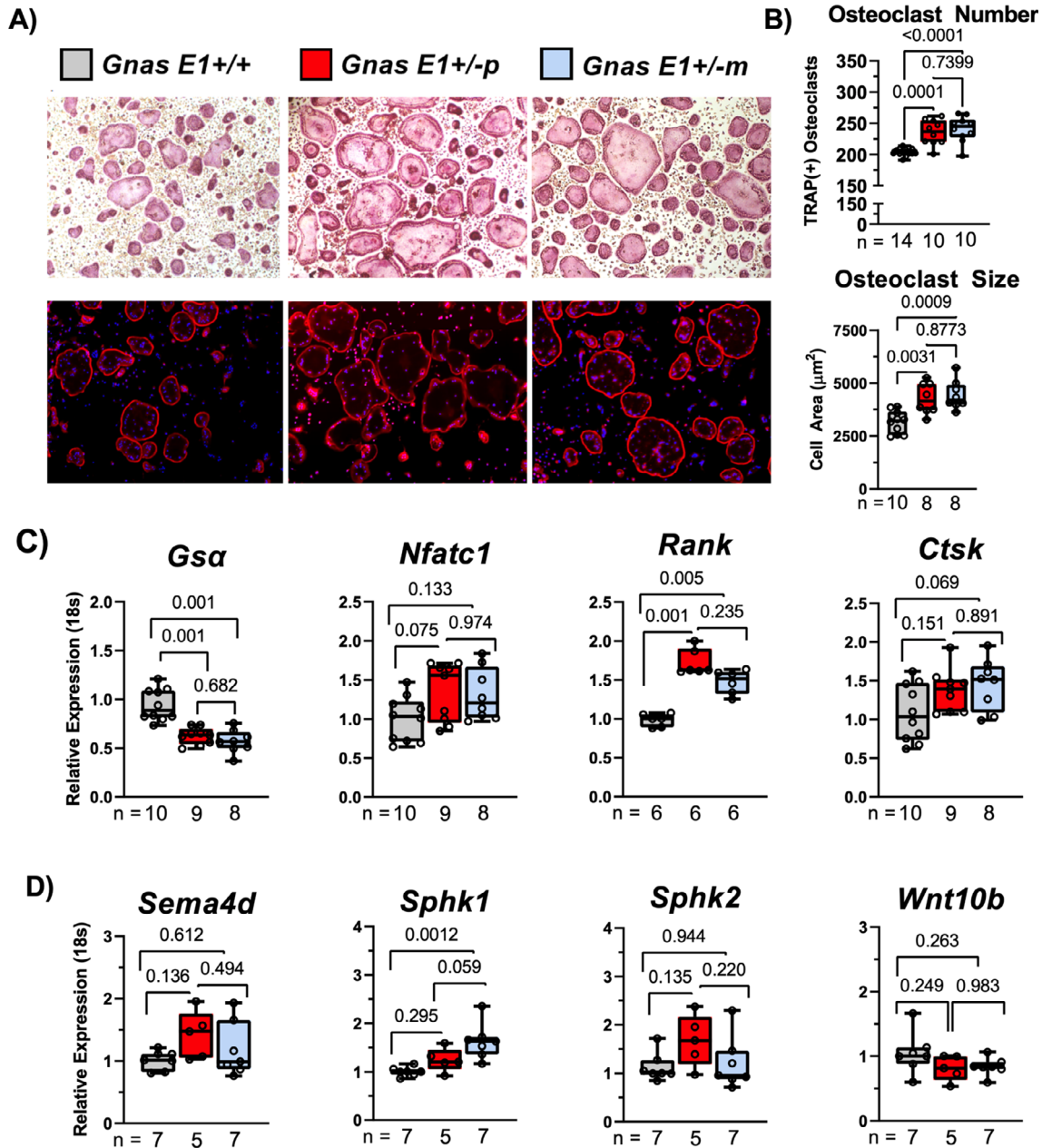
Fig 5. *Gnas E1+/−m* osteoclasts display elevated *Sphk1* expression in vitro. (*A*) Representative images of chromogenic TRAP staining (top) and phalloidin-DAPI fluorescence microscopy staining of primary BMM cultures (bottom) from male and female mice in vitro. (*B*) *Gnas E1+/−m* and *Gnas E1+/−p* demonstrated increased rates of osteoclastogenesis and osteoclast surface area compared to WT as indicated by increased osteoclast number following 5 days of differentiation. Osteoclasts were defined as TRAP(+) cells with ≥3 nuclei. No significant differences were observed in osteoclast number between *Gnas +/−p* and *Gnas +/−m* cultures, respectfully; (*C*) Gsα mRNA expression was significantly reduced in both *Gnas E1+/−m* and *Gnas E1+/−p* cultures when compared to WT. No significant variations were observed in mRNA expression of *Nfatc1* or *Ctsk* among *Gnas E1+/−* cultures and WT at day 5 of osteoclast differentiation. However, both *Gnas E1+/−p* and *Gnas E1+/−m* cultures demonstrated a significant increase in *Rank* expression compared to WT. (*D*) *Gnas E1+/−m* cultures display significantly elevated *Sphk1* mRNA expression when compared to WT cultures. Sample size per genotype per experiment is listed on each bar graph. All statistical tests completed using ANOVA with post-hoc Tukey test for multiple comparisons, and *p* values are displayed for each comparison.

measurements, female *Gnas E1+/−p* mice displayed a significant increase in the ratio of osteoclast surface to bone surface (Oc.S/BS) when compared to both WT and *Gnas E1+/−m* mice, whereas *Gnas E1+/−m* mice displayed no significant

variations in Oc.S/BS when compared to WT (Fig. 6E). Additionally, female *Gnas E1+/−p* mice displayed a significant increase in the number of osteoclasts per bone surface (N. Oc/BS) when compared to WT, whereas *Gnas E1+/−m* mice
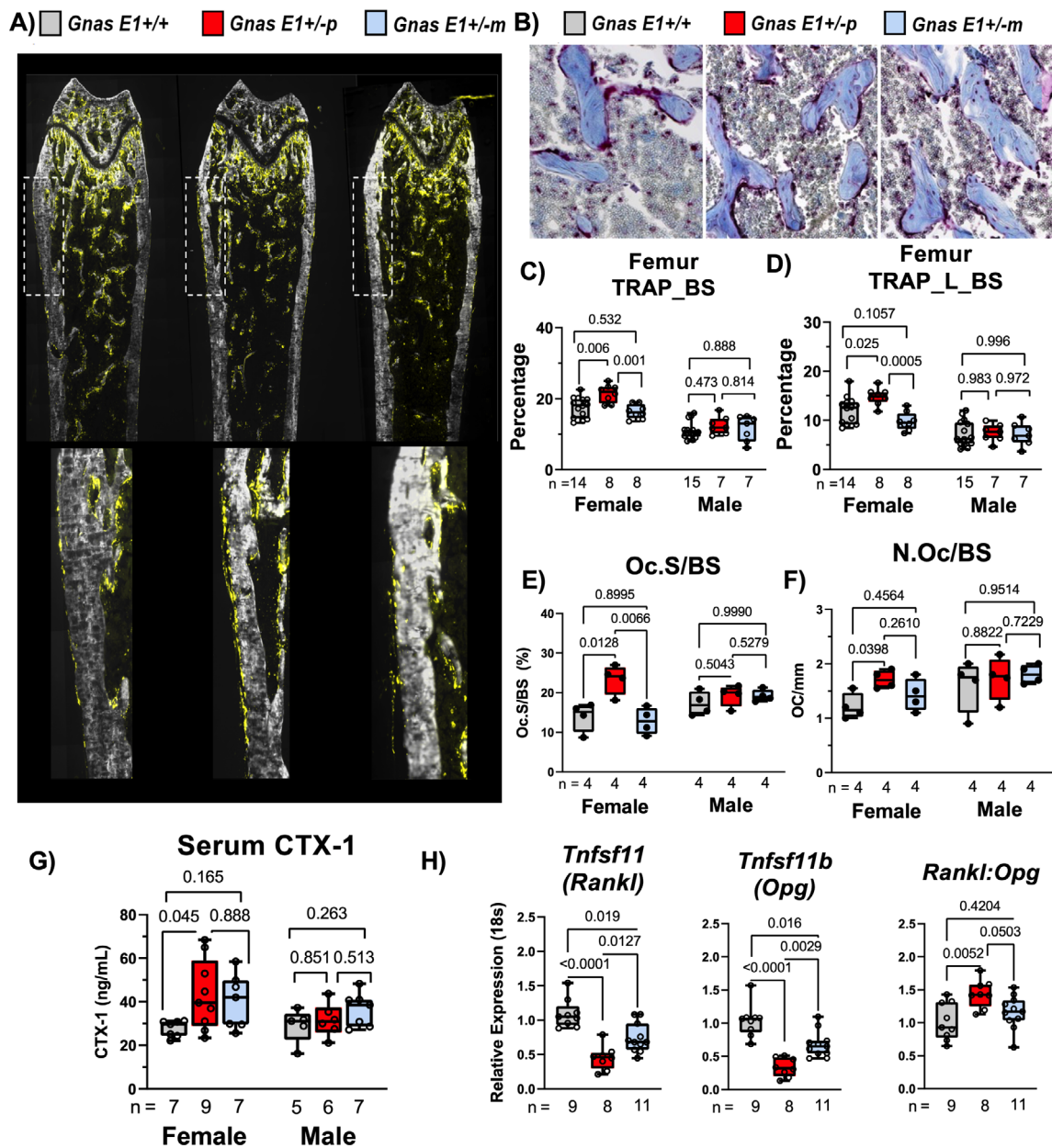
Fig 6. *Gsα* heterozygous inactivation differentially affects bone resorption in a parental inheritance-specific pattern in vivo. (*A*) Representative images of undecalcified distal femur sections demonstrating TRAP enzymatic activity on the bone surface (TRAP_BS) following incubation with Elf97 fluorescent substrate. (*B*) Representative images of distal femur trabeculae stained with TRAP for visualization of osteoclasts on the bone surface; counterstained with aniline blue. (*C,D*) Female *Gnas E1*+/−*p* mice demonstrated a significant increase in (*C*) total TRAP activity on the bone surface (TRAP_BS) and (*D*) active bone remodeling sites (TRAP_L_BS) within the femur when compared to WT and *Gnas E1*+/−*m* mice. No significant variations were observed between female *Gnas E1*+/−*m* and WT mice. No significant phenotype was observed within male mice. (*E*) Chromogenic TRAP staining revealed female *Gnas E1*+/−*p* mice demonstrated a significant increase in the ratio of osteoclast surface/bone surface when compared to both WT and *Gnas E1*+/−*m* mice. No significant variations were observed between female *Gnas E1*+/−*m* and WT mice. No significant phenotype was observed within male mice. (*F*) Female *Gnas E1*+/−*p* mice displayed a significant increase in the number of osteoclasts per bone surface when compared to WT mice. No significant variations were observed between female *Gnas E1*+/−*m* and WT mice or between *Gnas E1*+/−*m* and *Gnas E1*+/−*p* mice. No significant phenotype was observed within male mice. (*G*) Female *Gnas E1*+/−*p* mice displayed significantly elevated fasting serum CTX-1 measurements when compared to WT. (*H*) RT-PCR analysis of flushed tibia diaphysis from male and female mice identified both *Gnas E1*+/−*p* and *Gnas E1*+/−*m* mice had reduced mRNA expression of *Tnfsf11* (Rankl) and *Tnfsf11b* (Opg) when compared to WT. *Gnas E1*+/−*m* mice displayed significantly increased *Rankl* and *Opg* mRNA expression when compared to *Gnas E1*+/−*p*. However, *Gnas E1*+/−*p* mice displayed a significantly elevated *Rankl:Opg* ratio when compared to WT but were not statistically significant when compared to *Gnas E1*+/−*m* mice. Sample size per genotype per experiment is listed on each bar graph. All statistical tests completed using ANOVA with post-hoc Tukey test for multiple comparisons, and *p* values are displayed for each comparison.

displayed no significant variations in N.Oc/BS when compared to WT (Fig. 6F). No significant variations in Oc.S/BS or N.Oc/BS activity were observed within male mice (Fig. 6E,F). Within the lumbar vertebrae, *Gnas E1+/−p* mice displayed an elevated TRAP_BS when compared to WT and had an elevated TRAP_L_BS when compared to both WT and *Gnas E1+/−m* mice (Supplemental Fig. S1E,F). Complementary to these histomorphometry findings, female *Gnas E1+/−p* mice displayed significantly elevated serum CTX-1 compared to WT (Fig. 6G), whereas no significant changes were observed in *Gnas E1+/−m* serum levels. Additionally, no significant variations were observed between *Gnas E1+/−p* and *Gnas E1+/−m* measurements. These data correlate with previous reports in

the literature that demonstrate enhanced osteoclast activity specifically among *Gnas E1+/−p* mice.[44]

Quantitative RT-PCR from tibia specimens isolated from both male and female mice revealed that *Gnas E1+/−p* and *Gnas E1+/−m* mice displayed a significant reduction in both *Rankl* and *Opg* (Fig. 6H) mRNA expression when compared to WT. Despite both *Rankl* and *Opg* being downregulated in *Gnas E1+/−* mice, *Gnas E1+/−p* mice observed a more significant reduction in *Opg* expression when compared to *Rankl* reduction, which directly correlates with previous tibial and calvaria mRNA data in the literature from *Gsα*-deficient animals.[36,37] Consequently, this resulted in *Gnas E1+/−p* mice displaying an elevated *Rankl:Opg* ratio (Fig. 6H) when
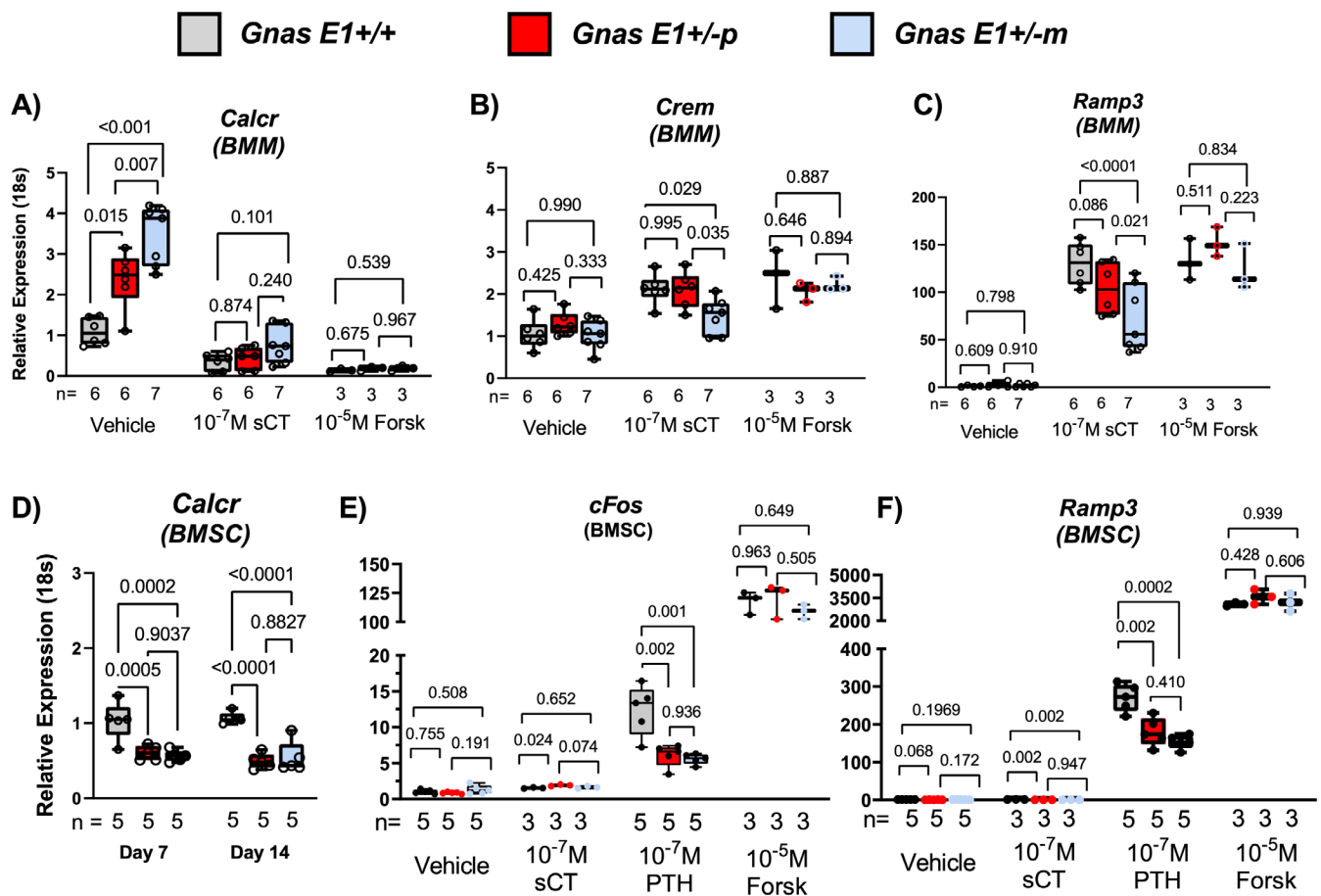

Fig 7. *Gnas E1+/−m* osteoclasts display impaired calcitonin receptor bioactivity in vitro. (A) *Gnas E1+/−m* and *Gnas E1+/−p* osteoclasts displayed significant elevations in *Calcr* mRNA expression when compared to WT; however, *Calcr* expression within *Gnas E1+/−m* cultures was significantly greater than *Gnas E1+/−p* cultures. Treatment of *Gnas E1+/−* and WT osteoclasts with 1×10^{-7}M sCT or 1×10^{-5}M forskolin resulted in significant reductions in *Calcr* expression. (B,C) RT-PCR analysis of *Crem* and *Ramp3* mRNA expression of *Gnas E1+/−m*, *Gnas E1+/−p*, and WT cultures following exposure to sCT or vehicle controls for 6 hours. sCT-treated *Gnas E1+/−m* cultures displayed a significant reduction in *Crem* and *Ramp3* mRNA expression compared to *Gnas E1+/−p* and WT sCT-treated cultures. No significant variations in *Crem* or *Ramp3* expression were observed between *Gnas E1+/−p* and WT sCT treated cultures. (D) *Gnas E1+/−m* and *Gnas E1+/−p* BMSCs following 7 and 14 days of osteogenic differentiation demonstrate a significant reduction in *Calcr* mRNA expression when compare to WT. (E,F) RT-PCR analysis of c-Fos and *Ramp3* mRNA expression of *Gnas E1+/−m*, *Gnas E1+/−p*, and WT BMSCs following exposure to sCT, PTH, forskolin, or vehicle controls for 6 hours. BMSCs overall displayed no significant response to sCT treatment. However, *Gnas E1+/−m* and *Gnas E1+/−p* BMSCs displayed a reduction in c-Fos and *Ramp3* when compared to WT BMSCs following PTH treatment. No significant variations in c-Fos or *Ramp3* expression were observed between PTH treated *Gnas E1+/−m* and *Gnas E1+/−p* BMSCs. Sample size per genotype per experiment is listed on each bar graph. All statistical tests completed using two-way ANOVA with post-hoc Tukey test for multiple comparisons, and p values are displayed for each comparison. sCT = salmon calcitonin.

compared to WT. *Gnas E1+/−m* mice exhibited a more modest reduction in both *Rankl* and *Opg* expression when compared to WT, with no significant change in the *Rankl:Opg* ratio. Collectively, despite *Gnas E1+/−m* and *Gnas E1+/−p* mice displaying equally elevated rates of osteoclastogenesis in vitro, only *Gnas E1+/−p* mice show elevated bone resorption activity in vivo. These data show that the reduced cortical and trabecular bone parameters within *Gnas E1+/−p* mice are driven by a combination elevated resorption activity specifically within *Gnas E1+/−p* mice, in conjunction with their impaired bone formation activity.

Inheritance-specific variations in bioactivity of Gsα-coupled receptors are observed in calcitonin signaling within the osteoclast lineage among *Gnas E1+/−* mice in vitro

In light of these distinctions in bone remodeling among *Gnas E1+/−m* and *Gnas E1+/−p* mice, we next sought to identify whether these differences could be driven by changes in bioactivity of Gsα-coupled receptors within specific cell-types in the bone microenvironment. Although multiple hormones have been identified to influence bone homeostasis through Gsα-mediated signaling, we were particularly interested in comparing the responsiveness of osteoclasts to the hormone calcitonin, as well as observing the responsiveness of osteoblasts to PTH. It has been well-described that patients with PHP1A can manifest resistance to calcitonin.[54,55] In primary BMM cultures, we observed a significant upregulation in Calcitonin receptor (*Calcr*) mRNA expression in both *Gnas E1+/−m* and *Gnas E1+/−p* cells compared to WT (Fig. 7A). Given that *Calcr* is an often-utilized transcriptional marker of mature osteoclasts in vitro, this finding was anticipated based upon the increased rates of osteoclastogenesis in both *Gnas E1+/−m* and *Gnas E1+/−p* cultures. However, *Gnas E1+/−m* primary cultures also displayed a consistent upregulation of *Calcr* expression when compared to *Gnas E1+/−p* cultures despite having similar numbers of osteoclasts in vitro (Fig. 7A).

Within the osteoclast, the transcriptional activity of *Calcr* is maintained through a negative autoregulatory feedback loop based upon calcitonin receptor activation.[56,57] We therefore wanted to address whether the observed upregulation in *Calcr* expression specifically within *Gnas E1+/−m* cultures was attributed to impaired calcitonin receptor Gsα-mediated signaling. *Gnas E1+/−m*, *Gnas E1+/−p*, and WT BMMs were treated with 1×10^{-7}M sCT (R&D Systems) to activate Gsα signaling, with 1×10^{-5}M forskolin (Sigma-Aldrich) to activate adenylyl cyclase (AC) downstream of Gsα, or with vehicle controls (PBS) for 6 hours. We monitored calcitonin receptor bioactivity by quantitative RT-PCR analysis of *Calcr*, as well as *Crem* and *Ramp3*. These two additional genes were selected because their transcriptional activity has been shown to be directly influenced by signaling through Gsα-coupled receptors and have previously been validated to monitor the responsiveness of osteoclasts to calcitonin in vitro.[48,58] Exposure of WT, *Gnas E1+/−p*, and *Gnas E1+/−m* cultures to sCT and forskolin resulted in a reduction of *Calcr* mRNA expression when compared to vehicle-treated cultures (Fig. 7A). We did not observe any statistically significant variations in *Calcr* expression among sCT-treated cultures. *Gnas E1+/−m* osteoclast cultures treated with sCT displayed a significant reduction of both *Crem* (Fig. 7B) and *Ramp3* (Fig. 7C) mRNA expression when compared to both WT and *Gnas E1+/−p* sCT-treated cultures, as well as forskolin-treated *Gnas E1+/−m*

cultures. Both *Crem* and *Ramp3* mRNA expression levels in *Gnas E1+/−p* cultures following sCT treatment were comparable to WT. In addition, treatment of cultures with forskolin displayed no significant variations in *Crem* or *Ramp3* mRNA expression between *Gnas E1+/−* –treated or WT-treated cultures. Therefore, these data suggest evidence of partial calcitonin resistance within *Gnas E1+/−m* osteoclasts in vitro and imply that this reduced activity is driven specifically by impaired calcitonin receptor Gsα-mediated signaling. Although we did not observe any variations in Gsα transcription between *Gnas E1+/−p* and *Gnas E1+/−m* BMM cultures in vitro (Fig. 5C), these statistical changes in calcitonin-receptor bioactivity may be reflective of a preferential targeting of osteoclasts within this mixed culture system and further investigations are necessary.

Biallelic expression of *Gsα* within the osteoblast lineage in *Gnas E1+/−* mice in vitro

Given these distinctions in *Calcr* mRNA expression and receptor bioactivity in osteoclast cultures, we subsequently evaluated *Calcr* expression within BMSCs following 7 and 14 days of osteogenic differentiation (Fig. 7D), as well as in flushed tibia samples (Supplemental Fig. S2A). We observed that BMSCs from *Gnas E1+/−m* and *Gnas E1+/−p* mice displayed significant reductions in *Calcr* mRNA expression when compared to WT after 7 and 14 days of osteogenic differentiation (Fig. 7D). Similarly, flushed tibia samples from *Gnas E1+/−m* and *Gnas E1+/−p* mice displayed significant reductions in *Calcr* mRNA expression when compared to WT (Supplemental Fig. S2A). Although these data would suggest similarities in overall Gsα-receptor mediated signaling within the osteoblast, we wanted to more closely confirm this finding in vitro by exposing BMSCs isolated from *Gnas E1+/−* and WT mice that were treated for 14 days in osteogenic differentiation media to 1×10^{-7}M sCT (R&D Systems), 1×10^{-7}M PTH 1–34 (ProSpec), 1×10^{-5}M forskolin (Sigma-Aldrich), or vehicle controls (PBS) for 6 hours. We assessed the bioactivity of Gsα-coupled receptors within BMSCs by monitoring the mRNA expression of *c-Fos*, *Ramp3*, and *Crem*, which have been previously validated in the literature to identify Gsα-mediated signaling within BMSCs, particularly in response to treatment with PTH.[59] Treatment of both *Gnas E1+/−* and WT BMSCs with sCT resulted in no significant changes in *c-Fos* (Fig. 7E), *Ramp3* (Fig. 7F), or *Crem* (Supplemental Fig. S2B) expression when compared to vehicle treated cultures. This finding was expected based upon previous reports documenting an inability of osteoblasts to respond to calcitonin despite their mRNA expression of *Calcr*.[48,60] Treatment of *Gnas E1+/−* and WT BMSCs with forskolin resulted in a robust increase in *c-Fos*, *Ramp3*, and *Crem* expression when compared to vehicle-treated controls; additionally, no significant variations in mRNA expression were observed when comparing forskolin-treated *Gnas E1+/−m*, *Gnas E1+/−p*, and WT cultures. Treatment of *Gnas E1+/−* and WT BMSCs with PTH 1–34 also caused an upregulation in *Ramp3* and *cFos* mRNA expression when compared to vehicle-treated controls (Fig. 7E,F). Significant changes in *Crem* expression compared to vehicle controls were only observed in WT cultures (Supplemental Fig. S2B). When comparing PTH treated BMSCs, both *Gnas E1+/−m* and *Gnas E1+/−p* BMSCs displayed a significant reduction in both *c-Fos* and *Ramp3* mRNA expression when compared to WT. No significant variations in *Ramp3*, *cFos*, or *Crem* were observed when comparing *Gnas E1+/−p* to *Gnas E1+/−m* PTH-treated cultures. Collectively, the combination of similar reductions in *Gsα* and *Calcr* mRNA expression

between *Gnas E1+/−m* and *Gnas E1+/−p* BMSCs when compared to WT, in addition to both *Gnas E1+/−m* and *Gnas E1+/−p* BMSCs displaying impaired Gsα-mediated signaling following PTH treatment when compared to WT, suggest the presence of biallelic expression of Gsα within the osteoblast lineage.

Discussion

Our data provide direct evidence of distinct changes in cortical and trabecular bone architecture among adult *Gnas E1+/−* mice dependent upon the inheritance pattern of their mutation. Specifically, mice with maternally derived (*Gnas E1+/−m*) mutations display elevated cortical and trabecular bone parameters when compared to WT mice. We identified a direct correlation between these increased cortical and trabecular bone parameters and enhanced osteoblast activity (as measured by MAR and serum P1NP) within *Gnas E1+/−m* mice. These observations directly correlate with our previous findings of normal to increased BMD in PHP1A patients.[42] Alternatively, mice with paternally derived (*Gnas E1+/−p*) mutations displayed evidence of reduced cortical bone parameters when compared to both *Gnas E1+/−m* and WT mice. Similarly, *Gnas E1+/−p* mice displayed evidence of normal to reduced osteoblast activity in conjunction with elevated osteoclast activity in vivo. These observations in *Gnas E1+/−p* mice directly correlate with the previous findings in the literature suggesting that impaired Gsα signaling leads to an osteopenic bone phenotype.[36–41] These findings could have potential implications for patients with PPHP and have yet to be correlated.

Although histomorphometric analyses were performed using both male and female mice, we identified distinctions in both bone formation and bone resorption in female *Gnas E1+/−* mice, whereas male *Gnas E1+/−* mice only displayed variations in bone formation in vivo. This dimorphism is aligned with previous studies demonstrating that female mice display higher trabecular bone turnover and therefore may be more susceptible to phenotypic perturbations when compared to male mice.[61,62]

Our observations of enhanced osteoblast activity within *Gnas E1+/−m* mice vary from previous findings performed by Ramaswamy and colleagues[44] utilizing our AHO mouse model bred on a mixed 129SvEv × CD1 background. In this previous study, *Gnas E1+/−m* mice displayed a reduced MAR on the endocortical surface compared to littermate controls, whereas no significant differences were observed between *Gnas E1+/−p* and littermate controls.[44] It is first important to note that this histomorphometric analysis was performed on mice younger than the time point that we have evaluated (this previous study's analysis was performed at 2 weeks of age). Second, μCT analysis at 2 weeks revealed that both *Gnas E1+/−p* and *Gnas E1+/−m* mice displayed a reduced cortical thickness and cortical BV/TV when compared to littermate controls. This study performed additional μCT analysis at 3 months and displayed similar patterns in cortical bone parameters that we observed between *Gnas E1+/−p* and *Gnas E1+/−m* mice; however, no formal analysis of osteoblast number or function was performed past 2 weeks of age. Therefore, it is plausible that in the early phases of long-bone development, osteoblast activity is impaired within *Gnas E1+/−m* mice. However, following the initial stages of bone modeling, osteoblast activity specifically increases within *Gnas E1+/−m* mice due to changes within the local bone microenvironment, whereas osteoblast activity remains normal to reduced in *Gnas E1+/−p* mice.

We also identified elevated rates of osteoclastogenesis and increased osteoclast size within both *Gnas E1+/−m* and *Gnas E1+/−p* primary BMM cultures when compared to WT. RT-PCR analysis of mature osteoclast cultures identified that both *Gnas E1+/−p* and *Gnas E1+/−m* cultures showed significantly elevated mRNA expression of *Rank* and *Calcr* when compared to WT. These findings correlate with previous reports suggesting that *Gnas* serves as a negative regulator of osteoclastogenesis and osteoclast fusion[37,44,46]; therefore, it is plausible that *Gnas* or adenylate cyclase activity may serve a role in directly modulating the surface expression of RANK receptors within preosteoclasts, leading to elevated rates of osteoclastogenesis.[63,64]

Despite similar observations within *Gnas E1+/−m* and *Gnas E1+/−p* osteoclasts cultures in vitro, only *Gnas E1+/−p* mice displayed evidence of statistically enhanced osteoclast number and bone resorption activity when compared to WT in vivo as measured by histomorphometry and serum CTX-1 testing. *Gnas E1+/−m* mice displayed evidence of normal to slightly enhanced osteoclast activity compared to WT. We identified that both *Gnas E1+/−m* and *Gnas E1+/−p* mice displayed an overall reduction in total mRNA expression of both *Rankl* and *Opg* when compared to WT; however, *Gnas E1+/−p* mice displayed a significantly elevated *Rankl:Opg* mRNA expression ratio compared to WT due to a substantially greater reduction in *Opg* expression. *Gnas E1+/−m* mice maintained a *Rankl:Opg* ratio comparable to WT. This particular distinction was driven by the fact that *Gnas E1+/−m* displayed a more modest reduction in *Opg* mRNA expression when compared to *Gnas E1+/−p*. This relative difference in *Opg* expression provides an additional explanation into the distinct bone resorption findings among *Gnas E1+/−m* and *Gnas E1+/−p* mice in vivo. Additionally, given that OPG secretion is tightly regulated by osteoblast activity, it is possible that this distinction in bone resorptive activity may be secondary to an overall increase in osteoblast activity within *Gnas E1+/−m* mice.

When considering the imbalance within both osteoblast and osteoclast activity among *Gnas E1+/−m* and *Gnas E1+/−p* mice in vivo, we wanted to address whether these distinctions could be driven by inheritance-specific changes in Gsα mediated signaling within cell types involved in the bone remodeling process. Despite the observed changes in osteoblast activity in vivo, we observed no significant variations in Gsα expression, osteogenic differentiation or mineralization between *Gnas E1+/−m* and *Gnas E1+/−p* BMSCs when plated at equal cell densities in vitro. Although we identified variations in *Alpl*, *Sp7*, and *Bglap1* expression between *Gnas E1+/−m* and *Gnas E1+/−p* BMSCs, it is possible that these variations could have been the result of the heterogeneity of these cultures and the potential presence of contaminating osteoclasts within this system. Because of this, it is plausible that the transcriptional changes we observed could be reflective of potential variations in osteoblast–osteoclast interactions in vitro. In addition to observing no changes in osteogenic differentiation in vitro, both *Gnas E1+/−m* and *Gnas E1+/−p* mice similarly displayed an impaired bioactivity of Gsα-coupled receptors when primary BMSCs were treated with PTH 1–34 when compared to WT. These data correlate with previous findings that suggest evidence of Gsα biallelic expression within cells of the mesenchymal lineage and their differentiated states of adipocytes and chondrocytes.[19,26]

We also demonstrated that *Gnas E1+/−m* osteoclasts displayed impaired calcitonin receptor bioactivity when compared to both *Gnas E1+/−p* and WT cultures in vitro. We identified that this reduction in bioactivity was directly associated with

impaired Gsα-mediated signaling, given that supplementation of *Gnas E1+/−m* cultures with forskolin resulted in comparable expression of *Crem* and *Ramp3* when compared to WT and *Gnas E1+/−p* cultures. Although we did not observe any variations in *Gsα* transcription between *Gnas E1+/−p* and *Gnas E1+/−m* BMM cultures in vitro (Fig. 5C), these inheritance-specific variations in receptor activity, in conjunction with previous clinical reports of calcitonin-resistance in PHP1A, raise the possibility of partial *Gsα* imprinting within the mature osteoclast. Although the isolation of purified populations of mature osteoclasts has been a continual challenge within the field, a cluster of reports have recently described the potential of isolating purified populations from a mixed primary BMM culture system by the use of fluorescent reporter transgenic mouse models and fluorescence activated cell sorting (FACS).[65,66] The application of this emerging method in future studies is warranted, and these investigations could provide a more definitive insight into the prospect of differential *Gsα* expression within the mature osteoclast through genomic imprinting or through an unknown methylation-independent mechanism. These studies could also provide valuable insight into identifying further distinctions in cellular activity between *Gnas E1+/−p* and *Gnas E1+/−m* mice in both BMMs and osteoclasts that are independent of intracellular Gsα-signaling and instead potentially driven by concurrent hormonal resistance.

In addition to its role as an anti-resorptive pharmacologic target, the physiological role of the calcitonin receptor has gained interest, particularly with respect to its role in maintaining bone remodeling.[60] This interest has stemmed from the paradoxical phenotype that was observed in multiple reports showing that mice with global inactivation of *Calcr* display an elevated BV/TV and bone formation rate without any changes in total osteoblast or osteoclast number.[48,67] Additional studies of the lineage-specific deletion of *Calcr* revealed this anabolic phenotype in vivo was primarily driven by impaired calcitonin-receptor activity specifically within the osteoclast lineage (*LysM-CRE*) due to elevated sphingosine-1-phosphate (S1P) release.[48] Lineage-specific loss of *Calcr* within the mesenchymal lineage (*Runx2-CRE*), however, resulted in no phenotypic variations in bone architecture, osteoblast or osteoclast activity, or changes in S1P.[48] Interestingly, our data identified a significant reduction in *Calcr* mRNA expression in flushed tibia specimens as well as BMSC cultures within both *Gnas E1+/−m* and *Gnas E1+/−p* mice; however, only *Gnas E1+/−m* displayed impaired calcitonin receptor activity within the osteoclast lineage. *Gnas E1+/−m* osteoclasts also displayed a significantly elevated *Sphk1* expression when compared to WT cultures. Therefore, it is plausible that the observed distinctions in bone formation activity between *Gnas E1+/−m* and *Gnas E1+/−p* mice are driven by changes in sphingosine 1-phosphate (S1P) signaling by the osteoclast lineage due to calcitonin resistance. Although we did not observe any significant variations in plasma calcitonin measurements within *Gnas E1+/−m* mice (Supplemental Fig. S2C), the identification of spontaneous hypercalcitoninemia within PHP1A is not typically observed clinically.[55,68] Future provocative tests such as pentagastrin stimulation or sCT administration are warranted in order to assess the potential of this calcitonin receptor-S1P signaling axis influencing bone remodeling within *Gnas E1+/−m* mice in vivo. Additionally, further analysis of calcitonin and its role on both osteoclast function and osteoblast–osteoclast interaction within *Gnas E1+/−* mice is warranted in vitro through the use of co-culture studies of BMMs and osteoblasts isolated from WT, *Gnas E1+/−p*, and *Gnas E1+/−m* mice.

However, given the complexity of AHO, particularly with respect to the potential of other hormones also influencing the bone microenvironment within *Gnas E1+/−m* and *Gnas E1+/−p* mice, an unbiased and comprehensive genomewide analysis is also warranted to more definitively address this question.

In conclusion, our data are the first to show distinctions in bone remodeling between *Gnas E1+/−m* and *Gnas E1+/−p* mice and raise the potential of partial calcitonin resistance specifically within osteoclasts in *Gnas E1+/−m* mice. Moreover, these studies provide a potential etiology as to why we previously found that PHP1A patients display normal to increased bone mineral density.[42] In addition, we found evidence of distinctions in cortical and trabecular bone architecture that could directly impact patients with both PHP1A and PPHP. Further studies in patients with PPHP will be key in determining whether there are implications to overall bone health in terms of monitoring and treatment. Finally, these data also underscore that Gsα signaling not only influences bone remodeling by influencing cellular specific activities but also serves an essential role in modulating crosstalk between mesenchymal-lineage and myeloid-lineage cellular populations within the bone microenvironment.

Acknowledgments

Conflict of Interest

The authors declare that they have no disclosures or conflicts of interest.

Peer Review

The peer review history for this article is available at https://publons.com/publon/10.1002/jbm4.10570.

References

1. Albright F, Burnett C, Smith P. Pseudohypoparathyroidism: an example of "Seabright-Bantam syndrome.". *Endocrinology*. 1942;30: 922-932.

2. Albright F, Forbes A, Henneman P. Pseudo-pseudohypoparathyroidism. *Trans Assoc Am Physicians*. 1952;65:337-350.

3. Plagge A, Kelsey G, Germain-Lee EL. Physiological functions of the imprinted Gnas locus and its protein variants Gαs and XLαs in human and mouse. *J Endocrinol*. 2008;196(2):193-214.

4. Levine MA. An update on the clinical and molecular characteristics of pseudohypoparathyroidism. *Curr Opin Endocrinol Diabetes Obes*. 2012;19(6):443-451.

5. Germain-Lee EL. Management of pseudohypoparathyroidism. *Curr Opin Pediatr*. 2019;31(4):537-549.

6. Germain-Lee EL. Short stature, obesity, and growth hormone deficiency in pseudohypoparathyroidism type 1A. *Pediatr Endocrinol Rev*. 2006;3(2):318-327.

7. Levine MA. Chapter 64. Pseudohypoparathyroidism. *Principles of bone biology*. Academic Press; 2002 pp 1137-1163.

8. Linglart A, Levine MA, Jüppner H. Pseudohypoparathyroidism. *Endocrinol Metab Clin North Am*. 2018;47(4):865-888.

9. Levine MA, Germain-Lee E, De Beur SJ. Genetic basis for resistance to parathyroid hormone. *Horm Res*. 2003;60(Suppl 3):87-95.

10. Davies SJ, Hughes HE. Imprinting in Albright's hereditary osteodystrophy. *J Med Genet*. 1993;30(2):101-103.

11. Germain-Lee EL, Groman J, Crane JL, de Beur SM, Levine MA. Growth hormone deficiency in pseudohypoparathyroidism type 1a: another manifestation of multihormone resistance. *J Clin Endocrinol Metab*. 2003;88(9):4059-4069.

12. Levine MA, Downs RW, Moses AM, et al. Resistance to multiple hormones in patients with pseudohypoparathyroidism. Association with deficient activity of guanine nucleotide regulatory protein. *Am J Med*. 1983;74(4):545-556.

13. Bastepe M, Jüppner H. Editorial: pseudohypoparathyroidism and mechanisms of resistance toward multiple hormones: molecular evidence to clinical presentation. *J Clin Endocrinol Metab*. 2003;88(9): 4055-4058.

14. Germain-Lee EL, Ding C, Deng Z, et al. Paternal imprinting of Galpha(s) in the human thyroid as the basis of TSH resistance in pseudohypoparathyroidism type 1a. *Biochem Biophys Res Commun*. 2002; 296(1):67-72.

15. Namnoum AB, Merriam GR, Moses AM, Levine MA. Reproductive dysfunction in women with Albright's hereditary osteodystrophy1. *J Clin Endocrinol Metab*. 1998;83(3):824-829.

16. Mantovani G, Maghnie M, Weber G, et al. Growth hormone-releasing hormone resistance in pseudohypoparathyroidism type Ia: new evidence for imprinting of the Gsα gene. *J Clin Endocrinol Metab*. 2003; 88(9):4070-4074.

17. Mantovani G, Ballare E, Giammona E, Beck-Peccoz P, Spada A. The Gsα gene: predominant maternal origin of transcription in human thyroid gland and gonads. *J Clin Endocrinol Metab*. 2002;87(10): 4736-4740.

18. Liu J, Erlichman B, Weinstein LS. The stimulatory G protein α-subunit Gsα is imprinted in human thyroid glands: implications for thyroid function in pseudohypoparathyroidism types 1A and 1B. *J Clin Endocrinol Metab*. 2003;88(9):4336-4341.

19. Germain-Lee EL, Schwindinger W, Crane JL, et al. A mouse model of Albright hereditary osteodystrophy generated by targeted disruption of exon 1 of the Gnas gene. *Endocrinology*. 2005;146(11):4697-4709.

20. Long DN, McGuire S, Levine MA, Weinstein LS, Germain-Lee EL. Body mass index differences in pseudohypoparathyroidism type 1a versus pseudopseudohypoparathyroidism may implicate paternal imprinting of Gαs in the development of human obesity. *J Clin Endocrinol Metab*. 2007;92(3):1073-1079.

21. Hayward BE, Kamiya M, Strain L, et al. The human GNAS1 gene is imprinted and encodes distinct paternally and biallelically expressed G proteins. *Proc Natl Acad Sci U S A*. 1998;95(17):10038-10043.

22. Weinstein LS, Yu S, Ecelbarger CA. Variable imprinting of the heterotrimeric G protein G(S) α-subunit within different segments of the nephron. *Am J Physiol Renal Physiol*. 2000;278(4):F507-14.

23. Yu S, Yu D, Lee E, et al. Variable and tissue-specific hormone resistance in heterotrimeric Gs protein α-subunit (Gsα) knockout mice is due to tissue-specific imprinting of the Gsα gene. *Proc Natl Acad Sci U S A*. 1998;95(15):8715-8720.

24. Chen M, Shrestha YB, Podyma B, et al. Gsα deficiency in the dorsomedial hypothalamus underlies obesity associated with Gsα mutations. *J Clin Invest*. 2017;127(2):500-510.

25. Podyma B, Sun H, Wilson EA, et al. The stimulatory G protein Gsα is required in melanocortin 4 receptor–expressing cells for normal energy balance, thermogenesis, and glucose metabolism. *J Biol Chem*. 2018;293(28):10993-11005.

26. Sakamoto A, Chen M, Kobayashi T, Kronenberg HM, Weinstein LS. Chondrocyte-specific knockout of the G protein G(s)alpha leads to epiphyseal and growth plate abnormalities and ectopic chondrocyte formation. *J Bone Miner Res*. 2005;20(4):663-671.

27. Mantovani G, Bondioni S, Locatelli M, et al. Biallelic expression of the Gsalpha gene in human bone and adipose tissue. *J Clin Endocrinol Metab*. 2004;89(12):6316-6319.

28. Levine MA, Eil C, Downs RW, Spiegel AM. Deficient guanine nucleotide regulatory unit activity in cultured fibroblast membranes from patients with pseudohypoparathyroidism type I. A cause of impaired synthesis of 3′,5′-cyclic AMP by intact and broken cells. *J Clin Invest*. 1983;72(1):316-324.

29. Chen M, Gavrilova O, Liu J, et al. Alternative Gnas gene products have opposite effects on glucose and lipid metabolism. *Proc Natl Acad Sci U S A*. 2005;102(20):7386-7391.

30. Bastepe M, Weinstein LS, Ogata N, et al. Stimulatory G protein directly regulates hypertrophic differentiation of growth plate cartilage in vivo. *Proc Natl Acad Sci U S A*. 2004;101(41):14794-14799.

31. Kobayashi T, Soegiarto DW, Yang Y, et al. Indian hedgehog stimulates periarticular chondrocyte differentiation to regulate growth plate length independently of PTHrP. *J Clin Invest*. 2005;115(7):1734-1742.

32. Huso DL, Edie S, Levine MA, et al. Heterotopic ossifications in a mouse model of albright hereditary osteodystrophy. *PLoS One*. 2011;6(6): e21755.

33. Salemi P, Olson JMS, Dickson LE, Germain-Lee EL. Ossifications in Albright hereditary osteodystrophy: role of genotype, inheritance, sex, age, hormonal status, and BMI. *J Clin Endocrinol Metab*. 2018; 103(1):158-168.

34. Regard JB, Malhotra D, Gvozdenovic-Jeremic J, et al. Activation of Hedgehog signaling by loss of GNAS causes heterotopic ossification. *Nat Med*. 2013;19(11):1505-1512.

35. Pignolo RJ, Xu M, Russell E, et al. Heterozygous inactivation of Gnas in adipose-derived mesenchymal progenitor cells enhances osteoblast differentiation and promotes heterotopic ossification. *J Bone Miner Res*. 2011;26(11):2647-2655.

36. Sakamoto A, Chen M, Nakamura T, Xie T, Karsenty G, Weinstein LS. Deficiency of the G-protein α-subunit Gsα in osteoblasts leads to differential effects on trabecular and cortical bone. *J Biol Chem*. 2005; 280(22):21369-21375.

37. Xu R, Khan SK, Zhou T, et al. Gαs signaling controls intramembranous ossification during cranial bone development by regulating both Hedgehog and Wnt/β-catenin signaling. *Bone Res*. 2018;6(1):33.

38. Cong Q, Xu R, Yang Y. Gαs signaling in skeletal development, homeostasis and diseases. *Curr Top Dev Biol*. 2019;133:281-307.

39. Wu JY, Aarnisalo P, Bastepe M, et al. Gsα enhances commitment of mesenchymal progenitors to the osteoblast lineage but restrains osteoblast differentiation in mice. *J Clin Invest*. 2011;121(9):3492-3504.

40. Fulzele K, Krause DS, Panaroni C, et al. Myelopoiesis is regulated by osteocytes through Gsα-dependent signaling. *Blood*. 2013;121(6): 930-939.

41. Fulzele K, Dedic C, Lai F, et al. Loss of Gsα in osteocytes leads to osteopenia due to sclerostin induced suppression of osteoblast activity. *Bone*. 2018;117:138-148.

42. Long DN, Levine MA, Germain-Lee EL. Bone mineral density in pseudohypoparathyroidism type 1a. *J Clin Endocrinol Metab*. 2010;95(9): 4465-4475.

43. Schwindinger WF, Reese KJ, Lawler AM, Gearhart JD, Levine MA. Targeted disruption of Gnas in embryonic stem cells. *Endocrinology*. 1997;138(10):4058-4063.

44. Ramaswamy G, Kim H, Zhang D, et al. Gsα controls cortical bone quality by regulating osteoclast differentiation via cAMP/PKA and β-catenin pathways. *Sci Rep*. 2017;7:45140.

45. Hong S-HH, Jiang X, Chen L, Josh P, Shin D-GG, Rowe D. Computer-automated static, dynamic and cellular bone histomorphometry. *J Tissue Sci Eng*. 2012;5(1):4.

46. Ramaswamy G, Fong J, Brewer N, et al. Ablation of Gsα signaling in osteoclast progenitor cells adversely affects skeletal bone maintenance. *Bone*. 2018;109:86-90.

47. Yu J, Adapala NS, Doherty L, Sanjay A. Cbl-PI3K interaction regulates Cathepsin K secretion in osteoclasts. *Bone*. 2019;127:376-385.

48. Keller J, Catala-Lehnen P, Huebner AK, et al. Calcitonin controls bone formation by inhibiting the release of sphingosine 1-phosphate from osteoclasts. *Nat Commun*. 2014;5(1):5215.

49. Henriksen K, Karsdal MA, John Martin T. Osteoclast-derived coupling factors in bone remodeling. *Calcif Tissue Int*. 2014;94(1):88-97.

50. Sims NA, Martin TJ. Osteoclasts provide coupling signals to osteoblast lineage cells through multiple mechanisms. *Annu Rev Physiol*. 2020;82(1):507-529.

51. Lotinun S, Kiviranta R, Matsubara T, et al. Osteoclast-specific cathepsin K deletion stimulates S1P-dependent bone formation. *J Clin Invest*. 2013;123(2):666-681.

52. Pederson L, Ruan M, Westendorf JJ, Khosla S, Oursler MJ. Regulation of bone formation by osteoclasts involves Wnt/BMP signaling and the chemokine sphingosine-1-phosphate. *Proc Natl Acad Sci U S A*. 2008;105(52):20764-20769.

53. Dyment NA, Breidenbach AP, Schwartz AG, et al. Gdf5 progenitors give rise to fibrocartilage cells that mineralize via hedgehog signaling to form the zonal enthesis. *Dev Biol*. 2015;405(1):96-107.

54. Yavropoulou MP, Chronopoulos E, Trovas G, et al. Hypercalcitoninaemia in pseudohypo-parathyroidism type 1A and type 1B. *Endocrinol Diabetes Metab Case Rep*. 2019;2019:18-0125.

55. Vlaeminck-Guillem V, D'herbomez M, Pigny P, et al. Pseudohypoparathyroidism Ia and hypercalcitoninemia. *J Clin Endocrinol Metab*. 2001;86(7):3091-3096.

56. Granholm S, Lundberg P, Lerner UH. Expression of the calcitonin receptor, calcitonin receptor-like receptor, and receptor activity modifying proteins during osteoclast differentiation. *J Cell Biochem*. 2008;104(3):920-933.

57. Samura A, Wada S, Suda S, Iitaka M, Katayama S. Calcitonin receptor regulation and responsiveness to calcitonin in human osteoclast-like cells prepared in vitro using receptor activator of nuclear factor-κB ligand and macrophage colony-stimulating factor 1. *Endocrinology*. 2000;141(10):3774-3782.

58. Yang M, Kream BE. Calcitonin induces expression of the inducible cAMP early repressor in osteoclasts. *Endocrine*. 2008;33(3):245-253.

59. Estus TL, Choudhary S, Pilbeam CC. Prostaglandin-mediated inhibition of PTH-stimulated β-catenin signaling in osteoblasts by bone marrow macrophages. *Bone*. 2016;85:123-130.

60. Naot D, Musson DS, Cornish J. The activity of peptides of the calcitonin family in bone. *Physiol Rev*. 2019;99(1):781-805.

61. Rowe DW, Hong SH, Zhang C, et al. Skeletal screening IMPC/KOMP using μCT and computer automated cryohistology: application to the Efna4 KO mouse line. *Bone*. 2021;144:115688.

62. Mun SH, Jastrzebski S, Kalinowski J, et al. Sexual dimorphism in differentiating osteoclast precursors demonstrates enhanced inflammatory pathway activation in female cells. *J Bone Miner Res*. 2021; 36(6):1104-1116.

63. Weivoda MM, Ruan M, Hachfeld CM, et al. Wnt signaling inhibits osteoclast differentiation by activating canonical and noncanonical cAMP/PKA pathways. *J Bone Miner Res*. 2016;31(1):65-75.

64. Yoon SH, Ryu JY, Lee Y, Lee ZH, Kim HH. Adenylate cyclase and calmodulin-dependent kinase have opposite effects on osteoclastogenesis by regulating the PKA-NFATc1 pathway. *J Bone Miner Res*. 2011;26(6):1217-1229.

65. Madel M-B, Ibáñez L, Rouleau M, Wakkach A, Blin-Wakkach C. A novel reliable and efficient procedure for purification of mature osteoclasts allowing functional assays in mouse cells. *Front Immunol*. 2018;9: 2567.

66. Madel MB, Ibáñez L, Ciucci T, et al. Dissecting the phenotypic and functional heterogeneity of mouse inflammatory osteoclasts by the expression of cx3cr1. *Elife*. 2020;9:1-22.

67. Dacquin R, Davey RA, Laplace C, et al. Amylin inhibits bone resorption while the calcitonin receptor controls bone formation in vivo. *J Cell Biol*. 2004;164(4):509-514.

68. Mantovani G, Bastepe M, Monk D, et al. Diagnosis and management of pseudohypoparathyroidism and related disorders: first international consensus statement. *Nat Rev Endocrinol*. 2018;14(8): 476-500.